Virtual patients for mechanical ventilation in the intensive care unit

Computer Methods and Programs in Biomedicine 199 (2021) 105912

Contents lists available at ScienceDirect

Computer Methods and Programs in Biomedicine

journal homepage: www.elsevier.com/locate/cmpb

Virtual patients for mechanical ventilation in the intensive care unit

Cong Zhou[a,b], J. Geoffrey Chase[b,*], Jennifer Knopp[b], Qianhui Sun[b], Merryn Tawhai[c], Knut Möller[d], Serge J Heines[e], Dennis C. Bergmans[e], Geoffrey M. Shaw[f], Thomas Desaive[g]

[a] School of Civil Aviation, Northwestern Polytechnical University, China
[b] Department of Mechanical Engineering, University of Canterbury, New Zealand
[c] Auckland Bio-Engineering Institute (ABI), University of Auckland, New Zealand
[d] Institute for Technical Medicine, Furtwangen University, Villingen-Schwenningen, Germany
[e] Department of Intensive Care, School of Medicine, Maastricht University, Maastricht, the Netherlands
[f] Department of Intensive Care, Christchurch Hospital, Christchurch, New Zealand
[g] GIGA-In Silico Medicine, Institute of Physics, University of Liege, Liege, Belgium

ARTICLE INFO

Article history:
Received 1 October 2020
Accepted 12 December 2020

Keywords:
Hysteresis model
Hysteresis loop analysis
Digital twins
Virtual patient
Mechanical ventilation
Lung mechanics

ABSTRACT

Background: Mechanical ventilation (MV) is a core intensive care unit (ICU) therapy. Significant inter- and intra- patient variability in lung mechanics and condition makes managing MV difficult. Accurate prediction of patient-specific response to changes in MV settings would enable optimised, personalised, and more productive care, improving outcomes and reducing cost. This study develops a generalised digital clone model, or in-silico virtual patient, to accurately predict lung mechanics in response to changes in MV.

Methods: An identifiable, nonlinear hysteresis loop model (HLM) captures patient-specific lung dynamics identified from measured ventilator data. Identification and creation of the virtual patient model is fully automated using the hysteresis loop analysis (HLA) method to identify lung elastances from clinical data. Performance is evaluated using clinical data from 18 volume-control (VC) and 14 pressure-control (PC) ventilated patients who underwent step-wise recruitment maneuvers.

Results: Patient-specific virtual patient models accurately predict lung response for changes in PEEP up to 12 cmH_2O for both volume and pressure control cohorts. R^2 values for predicting peak inspiration pressure (PIP) and additional retained lung volume, V_{frc} in VC, are R^2=0.86 and R^2=0.90 for 106 predictions over 18 patients. For 14 PC patients and 84 predictions, predicting peak inspiratory volume (PIV) and V_{frc} yield R^2=0.86 and R^2=0.83. Absolute PIP, PIV and V_{frc} errors are relatively small.

Conclusions: Overall results validate the accuracy and versatility of the virtual patient model for capturing and predicting nonlinear changes in patient-specific lung mechanics. Accurate response prediction enables mechanically and physiologically relevant virtual patients to guide personalised and optimised MV therapy.

1. Introduction

Mechanical ventilation (MV) is a core therapy for respiratory failure and acute respiratory distress syndrome (ARDS) patients in the intensive care unit (ICU). However, non-optimal MV settings can cause ventilator induced lung injury (VILI), increasing length of stay, mortality and cost [1–4].

Titration of positive end-expiratory pressure (PEEP) [5] is one preferred way to keep alveoli open and improve oxygenation. However, determining the optimal PEEP for an individual patient is still unclear in clinical practice [6–9]. Lung protective strategies using a tidal volume of 6-8mL/kg [10,11] and plateau pressures under 30cmH_2O are well-accepted [10,12,13], although recent studies suggest the safe plateau pressure varies over time with patient condition, and airway pressure should thus be minimised [6,14–16]. However, sufficient PEEP is still needed to provide alveolar recruitment and adequate gas exchange.

Clinical evidence has reported both lower and/or higher PEEP ventilation reduces mortality in different subgroup analyses [16–20], confusing choices. It is clear optimal MV settings, particularly PEEP, have significant inter- and intra-individual variability. The ability to accurately monitor, capture, and predict the response

* Corresponding author.
E-mail address: Geoff.Chase@canterbury.ac.nz (J.G. Chase).

https://doi.org/10.1016/j.cmpb.2020.105912
0169-2607/

Abbreviations

HLA	Hysteresis loop analysis
HLM	Hysteresis loop model
MV	Mechanical ventilation
PC	Pressure Control or Pressure Controlled mechanical ventilation
PEEP	Positive end-expiratory pressure
PIP	Peak inspiratory pressure
RMs	Recruitment manoeuvres
RMS	Root-mean-square
V	Volume
VC	Volume Control or Volume Controlled mechanical ventilation
V_{frc}	Dynamic functional residual capacity volume gained or retained in the lung due to PEEP changes
V_{tidal}	Tidal volume
Variables	
V_{h1}	Volume associated with viscoelastic inspiratory hysteresis response
V_{h2}	Volume associated with viscoelastic expiratory hysteresis response
R	Airway resistance
K_e	Alveolar recruitment elastance
K_{e1}	Alveolar recruitment elastance at PEEP1
K_{h1}	Inspiratory nonlinear recruitment elastance
K_{h2}	Expiratory nonlinear recruitment elastance
K	Instantaneous elastance over time
V_{m1}	Lower inflection point
V_{m2}	Upper inflection point
δ	Controls the end-inspiratory stiffness
q	Controls the smoothness of end-inspiratory stiffness
K_c	Controls stiffness changes from inspiration to expiration
E_{m1}	Maximum inspiratory hysteresis energy
E_{h1}	Calculated inspiratory hysteresis energy
f_V	Input force
b	Coefficient for recruitment basis function
E	Coefficient for distention basis function
V_m	Upper limit tidal volume
α	post-yielding ratio
k_1	Identified HLA stiffness or elastance for the first inspiration segment as airways fill
k_2	Identified HLA stiffness or elastance for the second inspiration segment during recruitment
k_3	Identified HLA stiffness or elastance for the first expiration segment as airways release air
k_4	Identified HLA stiffness or elastance for the second expiration segment during derecruitment

to changing MV settings would offer insight and capability current care and equipment cannot provide.

An accurate, predictive virtual patient or digital clone based on a mechanical model of patient-specific lung mechanics would augment clinical data, provide a more comprehensive picture of patient-specific state, and predict response to care [21,22]. Accurate prediction enables more personalised, confident, and efficient MV delivery, minimising the risk of VILI, and could potentially reduce the length of MV, which is clinically and economically important [23].

Statistical models efficiently provide best mathematical combinations for predictive relationships, but offer little understanding of the underlying mechanics [24–27], even if prediction accuracy is acceptable [26,27]. A mechanical model offers more explicit meaning, physically and physiologically, and is thus more suitable for virtual patient models [25]. However, deterministic models can suffer from being too complex to identify or too simple for accuracy [25,28,29].

Currently, deterministic basis-function based virtual patient lung mechanics models provide accurate modelling and prediction using a linear single compartment lung model [30–32]. They assume the shape of lung elastance and resistance over pressure, volume and flow. This linear plus basis functions approach was taken over using the same model structure with nonlinear elements [33–38] for reasons of computational and identification simplicity. However, while effective, this basis function model approach lacks precision in fully capturing nonlinear lung mechanics, such as the added lung volume obtained when changing PEEP. Combining the single compartment lung model and the hysteresis loop analysis (HLA) method predicted airway pressure, but required parameters identified from multiple prior low PEEP steps [39], which is not clinically effective.

Finally, while lung mechanics models are common, predictive lung models are very limited. Mathematical models at cellular, tissue and geometric scales have enabled better understanding of lung mechanics [12,22,25,40–47]. However, they are complex, have many unknown parameters, and can suffer overfitting issues, excluding personalised model-based prediction. Hence, personalised models are less common, and predictive personalised models are very infrequent, as reviewed in [25,48].

This research presents a digital cloning method to create an accurate, predictive and patient-specific virtual patient model enabling personalised MV using a nonlinear, physiologically-relevant hysteresis loop model (HLM). It accurately captures lung mechanics, and predicts clinical important measured responses to changes in PEEP up to 12cmH_2O from a single PEEP level for both volume- and pressure-controlled (VC and PC) ventilation.

2. Methods

2.1. Hysteresis loop model (HLM) for lung respiratory mechanics

The key features to represent lung respiratory dynamics include the recruitment of alveoli and alveolar distension in inspiration, as well as the recoil of lung elastance in expiration. An identifiable HLM [49] is proposed with a linear spring, K_e, to represent the alveolar recruitment elastance, and two nonlinear hysteretic springs, K_{h1} and K_{h2}, for alveolar hysteresis elastance during inspiration and expiration, respectively. The proposed HLM is illustrated in Fig. 1.

The dynamic equation of motion for Fig. 1 is defined:

$$\ddot{V} + R\dot{V} + K_eV + K_{h1}V_{h1} + K_{h2}V_{h2} = f_V(t) + PEEP \tag{1}$$

where V is the volume of air delivered to the lungs, V_{h1} and V_{h2} are hysteretic volume response during inspiration and expiration, respectively, R is the airway resistance, PEEP is the positive end-expiratory pressure, and $f_V(t)$ is the steady-state input force.

The nonlinear stiffness, $K(t)$, for a breath can thus be defined in a differential form [49]:

$$K(t) = \frac{df_r}{dV} = K_e + K_{h1}\frac{\dot{V}_{h1}}{\dot{V}} + K_{h2}\frac{\dot{V}_{h2}}{\dot{V}} \tag{2}$$

where f_r is the total restoring force calculated from Eq. (1):

$$f_r(t) = f_V(t) - \ddot{V} - R\dot{V} + PEEP \tag{3}$$

Thus, the change of nonlinear stiffness is determined by the two hysteretic springs $K_{h1}\frac{\dot{V}_{h1}}{\dot{V}}$ and $K_{h2}\frac{\dot{V}_{h2}}{\dot{V}}$, giving the PV loop its characteristic shape in Fig. 1.

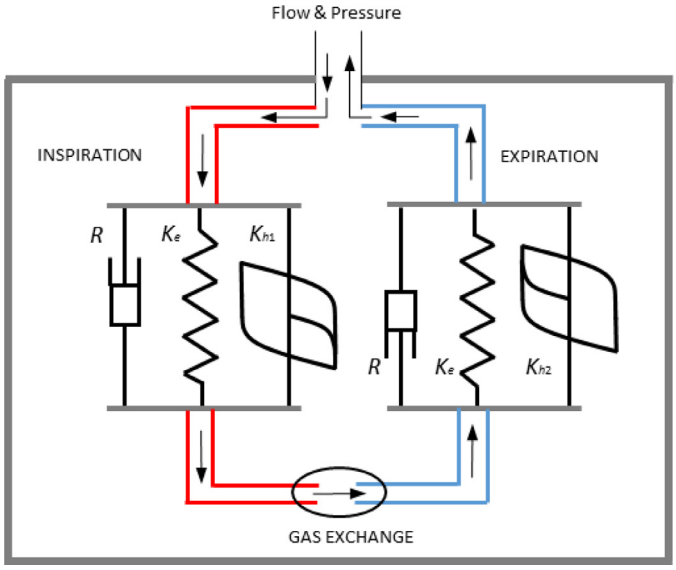

Fig. 1. Schematic diagram of the proposed HLM for lung mechanics.

In particular, the inspiratory hysteretic spring is defined:

$$\frac{\dot{V}_{h1}}{\dot{V}} = f_{sign}{}^{+}\left(1-\left(\frac{V_{h1}}{V_{m1}}\right)^{2}-\delta\left(\frac{E_{h1}}{E_{m1}}\right)^{q}\right)+K_c f_{sign}{}^{-} \tag{4}$$

where V_{m1} is the lower inflection point, δ controls the end-inspiratory stiffness due to distention or a pause, E_{h1} is the dissipated energy due to inspiratory hysteresis, q controls the smoothness of plateau stiffness, and E_{m1} is the maximum energy without inspiratory pause at peak alveolar pressure. K_c controls stiffness changes from inspiration to expiration via signum functions $f_{sign}{}^{+}$ and $f_{sign}{}^{-}$:

$$f_{sign}{}^{+} = 0.5 * \left(1+sign\left(V_{h1}\dot{V}\right)\right) \tag{5}$$

$$f_{sign}{}^{-} = 0.5 * \left(1-sign\left(V_{h1}\dot{V}\right)\right) \tag{6}$$

where $f_{sign}{}^{+} = 1$ in inspiration and $f_{sign}{}^{+} = 0$ in expiration, with $f_{sign}{}^{-} = 0$ and 1, respectively, thus asserting which term is active in Eq. (4).

The expiratory hysteretic spring is defined similarly to inspiration for alveolar derecruitment:

$$\frac{\dot{V}_{h2}}{\dot{V}} = f_{sign}{}^{-}\left(1-\left(\frac{V_{h2}}{V_{m2}}\right)^{2}\right) \tag{7}$$

where V_{m2} is the upper inflection point.

Therefore, ten (10) parameters, comprising: K_e, K_{h1}, K_{h2}, R, V_{m1}, V_{m2}, E_{m1}, K_c, q and δ, are defined to model the lung hysteresis mechanics using the proposed HLM. The input force, $f_V(t)$, also needs to be identified for model forward simulation. Fig. 2 shows the definition of HLM model parameters controlling the shape of a schematic PV loop.

2.2. Automated creation of a lung-mechanics virtual patient model

This section creates a virtual patient by identifying the proposed HLM parameters at a given PEEP to enable prediction of patient-specific lung dynamic response at higher or different PEEP levels. The identification process presented can be automated, requiring no human input, and includes:

- **Step1**: HLA identification of K_e, K_{h1}, K_{h2}, V_{m1}, V_{m2} and K_c;
- **Step2**: Calculation of R and f_V;

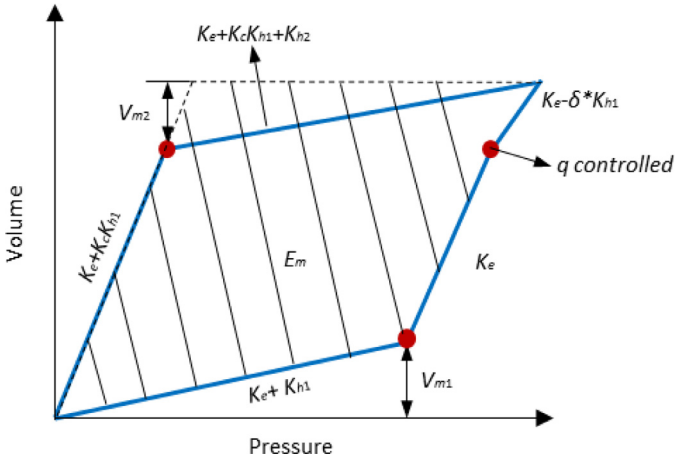

Fig. 2. Definition of HLM parameters in a schematic PV loop.

- **Step3**: Forward simulation of patient-specific response using the mechanics model identified from measured PV data at the given PEEP, to, in turn, use it to identify E_{m1} *and* q.

It is important to note that this proposed model is more directly identifiable [50,51] than more complex existing lung mechanics models [51–54].

2.2.1. Step1: HLA identification

HLA is an automated, well-proven algorithm for identifying the change of slopes and breakpoints for any general hysteresis loop [49,55–58]. The measured PV loop is divided into inspiratory and expiratory half cycles using the turning point T_{max} at maximum volume point (Fig. 3). The inspiration half cycle is approximated as two segments with HLA identified stiffness k_1, k_2 and the breakpoint V_{m1} for inspiration. HLA for the expiration half cycle yields k_3, k_4 and breakpoint V_{m2}.

The HLA identified stiffness values can be used to calculate model parameters K_e, K_{h1}, K_{h2} and K_c,:

$$K_e = k_2 = \alpha k_1 \tag{8}$$

$$K_{h1} = k_1 - k_2 \tag{9}$$

$$K_{h2} = k_3 - k_4 \tag{10}$$

$$K_c = \frac{k_4 - k_2}{k_1 - k_2} \tag{11}$$

The end-inspiratory parameter δ can then be calculated:

$$\delta = \frac{k_2 - k_{2end}}{k_1 - k_2} \tag{12}$$

where k_{2end} is the end-inspiratory stiffness identified in HLA shown in Fig. 3. Note, if $\delta<0$ distention exists, and $\delta>0$ captures an end-inspiratory pause.

2.2.2. Step2: Input force (f_V) and resistance (R)

The chest-lung system is assumed to be highly overdamped with relatively negligible higher frequency oscillation during breathing [59], as observed in clinical data. The volume changes for one breath cycle can be modelled using a steady-state harmonic input force:

$$f_V(t) = P_{amp}\sin(w * t + \varphi) \tag{13}$$

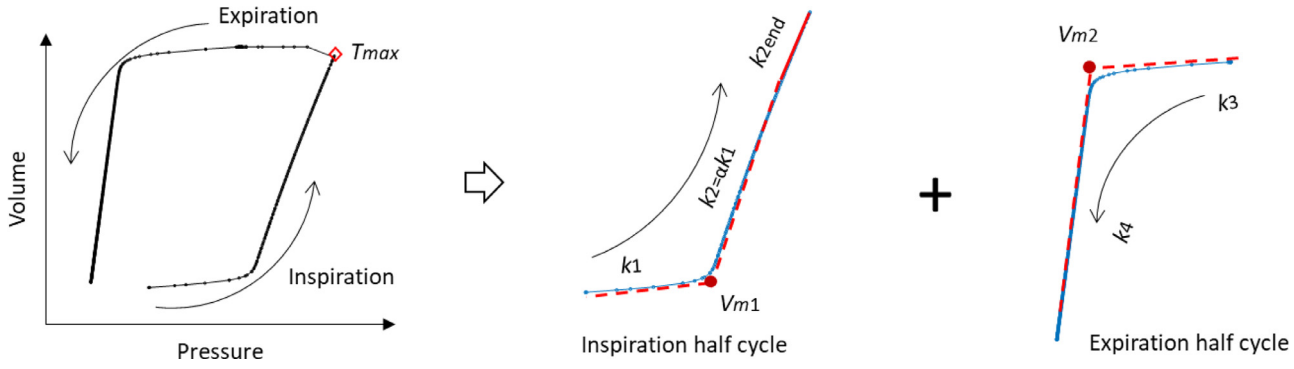

Fig. 3. HLA identification of a measured PV loop.

where the amplitude P_{amp} and phase φ can be calculated [60]:

$$P_{amp} = V_{tidal} * k\sqrt{\left(1 - \frac{w^2}{w_n^2}\right)^2 + \left(2\xi\frac{w}{w_n}\right)^2} \tag{14}$$

$$\varphi = tan^{-1}\frac{2\xi\,(w/w_n)}{1-(w/w_n)^2} \tag{15}$$

where V_{tidal} is the breathing tidal volume, and k is the equivalent initial inspiratory and expiratory filling (emptying) elastances estimated from:

$$k = \frac{1}{2}(k_1 + k_3) \tag{16}$$

A highly overdamped system is assumed with a large damping ratio ($\xi > 10$) eliminating the effect of free vibration or oscillation, which is not clinically observed in respiratory data. Thus, the volume attains its peak when the input force returns to zero, as seen at end inspiration, with the condition $w=w_n$, which gives $\varphi=\pi/2$. Eq. (14) can then be simplified and rewritten:

$$P_{amp} = 2\xi V_{tidal} k \tag{17}$$

The resistance parameter, R, in Eq. (1) can then be calculated:

$$R = 2\xi w = 2\xi\sqrt{k} \tag{18}$$

2.2.3. Step3: Forward simulation to find E_{m1} and q *in Eq. (4)*

The dissipated energy E_{h1} due to the nonlinear hysteresis force f_{h1} can be calculated [49]:

$$dE_{h1} = f_{h1}dV = K_{h1}V_{h1}dV \tag{19}$$

which yields:

$$E_{h1} = K_{h1}\int V_{h1}\dot{V}dt \tag{20}$$

Thus, the maximum energy parameter, E_{m1}, without considering distention, is obtained using forward simulation with the identified V_{m1}, K_e, K_{h1} and K_{h2} values found for the inspiratory half cycle in Step1.

The smoothness parameter, q, is found by minimizing normalized residual errors between the forward simulation and measurements during inspiration, using:

$$q = arg_{min}\sum_{i=1}^{n}\sqrt{\left(\frac{P_i - \hat{P}_i}{\bar{P}}\right)^2 + \left(\frac{V_i - \hat{V}_i}{\bar{V}}\right)^2} \tag{21}$$

where P and V are the measured pressure and volume, $\hat{P}$ and $\hat{V}$ are the modeled pressure and volume based on forward simulation of the identified model, and $\bar{P}$ and $\bar{V}$are the mean values of the measured pressure and volume (P and V), respectively.

2.3. Prediction using an identified virtual patient model

2.3.1. Prediction of K_e $(= k_2)$

In the identified HLM, the alveolar recruitment elastance, K_e (Fig. 2), is a key physiological feature whose changes capture the change of recruitment lung dynamics during a change of PEEP. Prior basis functions [30,31] have proven a good representation of observed mechanical lung behaviour during inspiration, considering the trade-off between alveolar recruitment and distention. In particular, linear and exponential shaped basis functions defined [31]:

$$E = E_1 * e^{bV} + E_2 * \frac{P}{60} \tag{22}$$

where E_1 is the coefficient for recruitment basis function and E_2 is the coefficient for distention basis function. V_m is the upper limit tidal volume and is set to 1L, while E_1 is equal to zero for $V > V_m$ [30,31].

Similarly, the same shape basis functions are employed to predict changes in the 'post-yielding' ratio, α, representing the change of stiffness from alveolar recruitment to distention in the HLM, as seen in Fig. 3, and defined:

$$\alpha = \frac{K_e}{k_1} = \frac{k_2}{k_1} = \alpha_1 * e^{b\frac{PEEP}{k_1}} + E * PEEP \tag{23}$$

where α_1 is the post-yielding ratio at the first low PEEP level, PEEP1, calculated:

$$\alpha_1 = \frac{K_{e1}}{k_1} \tag{24}$$

where K_{e1} is the identified value of K_e at PEEP1. In addition, the identified α_1 at the first low PEEP level, PEEP1, can provide:

$$\alpha_1 = \alpha_1 * e^{b\frac{PEEP1}{k_1}} + E * PEEP1 \tag{25}$$

For hysteresis behavior, the maximum possible value for the post-yielding ratio is $\alpha = 1$ [58] at the upper limit volume V_m, yielding:

$$E = \frac{1}{k_1 V_m} \tag{26}$$

Combining Eqs. (25) and (26) to solve b, yields:

$$b = \frac{k_1}{PEEP1}\log\frac{(\alpha_1 - EPEEP1)}{\alpha_1} \tag{27}$$

2.3.2. V_{frc} prediction

The predictive virtual patient model based on an identified, physiologically relevant HLM can simulate future changes of residual volume or functional residual capacity (V_{frc}) at the end of expiration when a change of PEEP level occurs. In particular, increasing

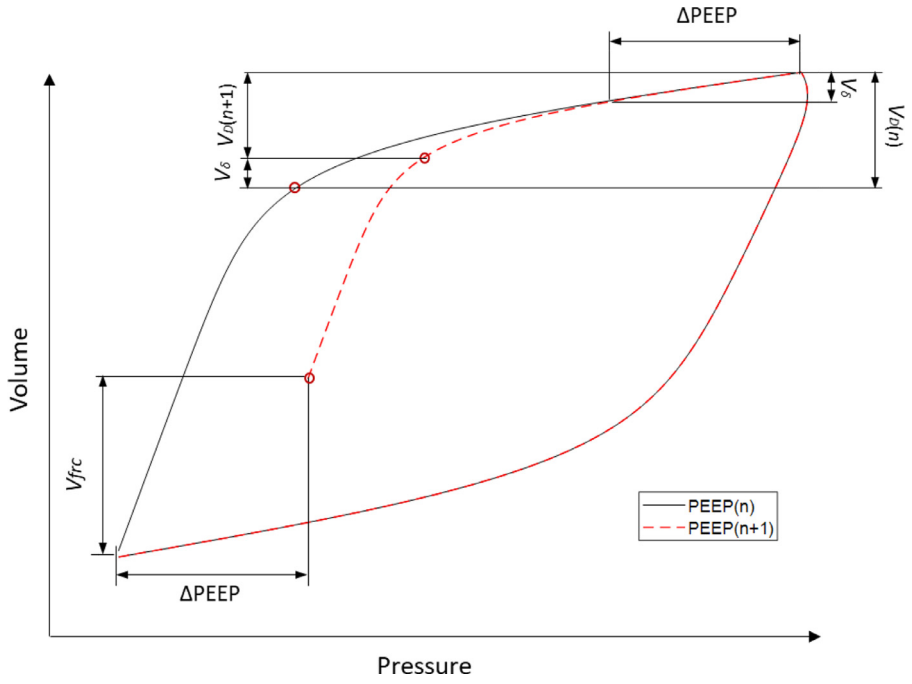

Fig. 4. Change of V_{frc} due to change of PEEP levels.

PEEP leads to an earlier end of expiration at a higher PEEP, retaining an additional lung volume, V_{frc}, as shown in Fig. 4. The resulting change of volume V_δ for ΔPEEP can be calculated:

$$V_\delta = \frac{\Delta PEEP}{k_3} = \frac{PEEP_{(n+1)} - PEEP_n}{k_3} \tag{28}$$

where k_3 is the alveolar decruitment stiffness identified in HLA in Step1 at $PEEP_n$ and is also held constant over all PEEP values (Fig. 3). Therefore, the breakpoint V_{m2} also changes with the change of volume drop V_δ, which can be described:

$$\frac{V_{m2}(PEEP_n)}{V_D} = \frac{V_{m2}\left(PEEP_{(n+1)}\right)}{V_D - V_\delta} \tag{29}$$

Combining Eqs. (28) and (29), the change of V_{m2} can be updated:

$$V_{m2}\left(PEEP_{(n+1)}\right) = V_{m2}(PEEP_n) - V_{m2}(PEEP_n)\frac{PEEP_{(n+1)} - PEEP_n}{V_D k_3} \tag{30}$$

Hence, the change of V_{frc} can be readily predicted by forward simulating the identified virtual patient model using the updated V_{m2} over PEEP changes, as shown schematically in Fig. 4.

2.4. Patient data

Clinical data includes 18 VC ventilated patients from the McREM trial in Germany and 14 PC ventilated patients from the Maastricht trial in Netherlands. Ethics approval for the McREM trial was granted by local ethics committee for each of the eight participating German ICUs [61]. The 14 patients in the Maastricht trail (METC17-4-053) [32] were treated using Bi-level Positive Airway Pressure (BIPAP), a common PC mode. Each patient in both cohorts underwent a 6-step staircase RM using ΔPEEP=2cmH2O/step, except Patient 18 in the McREM cohort who had only 4 steps. Pressure and flow data were recorded from the ventilators. Patient demographics for both cohorts are in Table 1.

Table 1
Patient demographics for both cohorts. Each cohort has 6 x ΔPEEP = 2 cmH2O RM increments from a base PEEP1 level (to PEEP2-7), except Patient 18 in the McREM cohort, which has 4 steps. There is thus a total of 190 predictions from PEEP1 to PEEP2-7 (106 for McREM and 84 for Maastricht).

McREM VC MV patient demographics (N=18)

Patient	Sex	Age	Clinical Diagnostic
1	Male	74	Subarachnoid and subdural hemorrhage
2	Female	50	Pancreatitis, pneumonia
3	Female	30	Peritonitis, sepsis
4	Female	49	Pneumonia
5	Male	34	Traumatic open brain injury
6	Male	67	Post resuscitation
7	Male	39	Perf. sigma, peritonitis
8	Male	42	Pneumonia, pancreatitis
9	Male	51	Traumatic brain injury, pneumonia
10	Male	77	Pneumonia
11	Male	37	Pneumonia
12	Male	41	Peritonitis
13	Male	62	Subarachnoid hemorrhage
14	Male	39	Traumatic brain injury, pneumonia
15	Male	74	S/P coronary artery bypass grafting, pneumonia
16	Male	59	ARDS
17	Male	45	Blunt abdominal trauma, pneumonia
18	Male	42	Acute GI bleeding, sepsis

Maastricht PC MV patient demographics (N=14)

Patient	Sex	Age	Clinical Diagnostic
1	Male	77	Coronary Artery Bypass Grafting
2	Female	85	Coronary Artery Bypass Grafting
3	Male	57	Coronary Artery Bypass Grafting
4	Male	47	Coronary Artery Bypass Grafting
5	Male	73	Aortic Valve Replacement
6	Male	75	Coronary Artery Bypass Grafting
7	Female	71	Aortic Valve Replacement
8	Male	76	Coronary Artery Bypass Grafting
9	Female	64	Subarachnoid Hemorrhage
10	Female	68	Pneumonia
11	Female	78	Pneumonia
12	Female	18	Mitral and Tricuspid Valve Replacement
13	Female	71	Pneumonia
14	Male	36	Coronary Artery Bypass Grafting

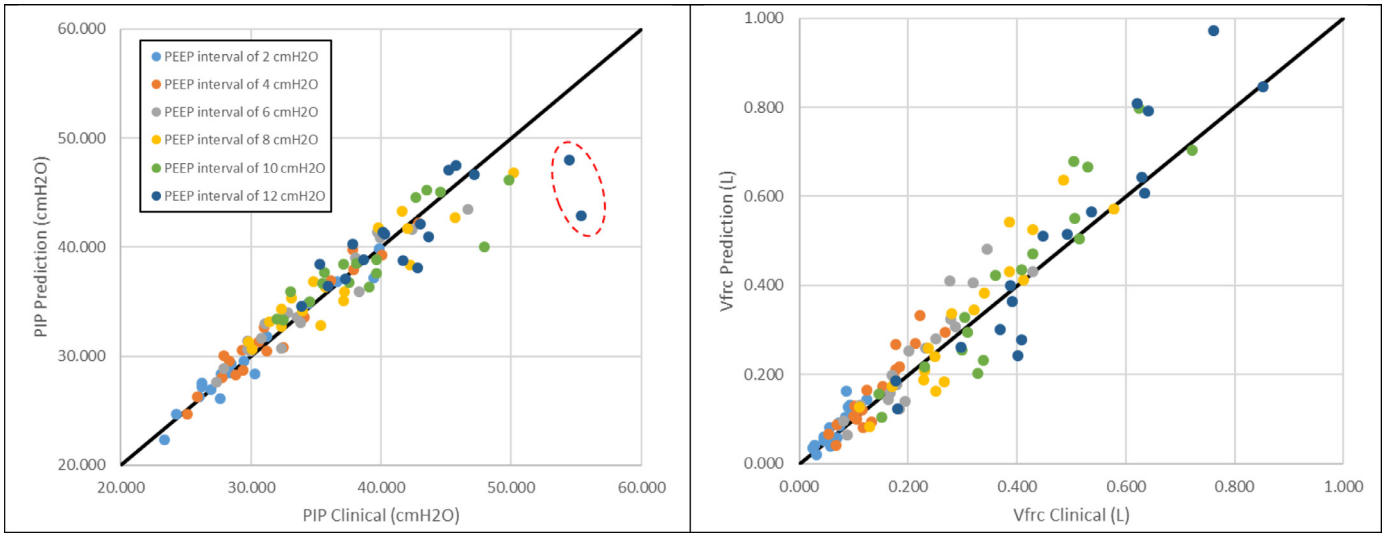

Fig. 5. McREM cohort prediction under VC MV for all patients and ΔPEEP prediction intervals (106 predictions). **Left**: Prediction of PIP with $R^2 = 0.86$, or $R^2 = 0.91$ for 104 predictions when excluding two outliers (circled) from one patient. **Right**: Prediction of V_{frc} with $R^2 = 0.90$.

2.5. Validation analyses

Validation uses the hysteresis PV loop at the starting PEEP level (PEEP1) to identify model parameters for the HLM and create the virtual patient model. Response is then predicted for all patients (N=32) at all higher PEEP levels over ΔPEEP intervals up to 12cmH2O (PEEP2-7; 6xPEEP steps), comprising 106 predictions for McREM VC patients and 84 for Maastricht PC patients.

Prediction results are compared using correlation plots with R^2 values for the 1:1 equivalence line, and error comparing clinically relevant measured and model predicted responses:

- Peak inspiratory pressure (PIP) absolute error (cmH2O) for volume-controlled McREM cohort;
- Peak inspiratory volume (PIV) absolute error (L) for pressure-controlled Maastricht cohort;
- V_{frc} absolute error (L).

Low prediction errors in these clinically relevant values would validate the model's ability to guide the design and delivery of safe, effective, patient-specific MV.

3. Results

Fig. 5 summarizes PIP and V_{frc} prediction results for the VC (McREM) cohort, showing very good PIP prediction with R^2=0.86 to the 1:1 perfect match line, increasing to R^2=0.91 with 2 outliers (~2%) from one patient excluded (circled). Predicted retained lung volume, V_{frc} compared to clinically measured V_{frc}, is very good with R^2=0.90. Overall, PIP prediction has median [IQR] error of 0.99 [0.55, 1.93]cmH2O and V_{frc} errors are 0.014 [0.006, 0.021]L with smaller errors at lower ΔPEEP intervals in Fig. 5. Appendices A-B have per-patient results.

Fig. 6 shows PIV and V_{frc} prediction for the PC (Maastricht) cohort, for 84 predicted cases over 14 patients. PIV prediction yields R^2 =0.86. Cumulative V_{frc}, prediction yields R^2=0.83 for all patients or R^2=0.91 excluding 3 outliers from the highest prediction intervals for 1 patient. Overall, PIV prediction has median [IQR] error of 0.030 [0.012, 0.049]L and V_{frc} errors are 0.016 [0.009, 0.032]L with smaller errors at lower ΔPEEP intervals in Fig. 6. Appendices C-D have per-patient results.

These results validate the ability of the virtual patient model to achieve good prediction for both VC and PC modes, and that it is robust across different patient conditions and both major ventilation modes. Accurate prediction for clinically-relevant changes and unrealistically high ΔPEEP is critical for clinical utility and full model validation, respectively, and is increasingly relevant in Covid-19 [62]. The HLM model is identified from clinical data using HLA combined with proven basis functions [30–32] for K_e to predict elastance evolution. Accurate prediction using only measurements from the current PEEP is unique in requiring no changes to PEEP to identify the model or perform prediction, as in [63,64], which also increases clinical validity.

Detailed individual per-patient prediction results are shown in Appendices A-D.

4. Discussion

A virtual patient model is identified at the lowest PEEP level (PEEP1) using the proposed HLM, and accurately predicts response at higher PEEP up to ΔPEEP=12cmH_2O for clinical validation. HLM model parameters are identified using the proven HLA method. A process requiring no human intervention makes it clinically applicable. It also avoids divergence and model mismatch issues found in nonlinear identification of similar hysteretic problems/models [50,65]. The overall results show very good accuracy in predicting clinically relevant peak values, V_{frc}, and patient-specific PV loops.

A more complex model with more nonlinear elements in the HLM might improve accuracy. However, identifiability and ability to automate identification would be reduced [25,50]. Equally, relatively higher accuracy with a more complex model is not necessarily more clinically useful. In particular, there are many models of lung mechanics, particularly at multiple scales, levels of linearity, and complexity [12,22,25,40–47], but while they match dynamics well, only a very few are predictive of outcome PV loops and mechanics, especially from a single breath, as reviewed in [25,48]. Thus, the utility of adding further nonlinear HLM model elements might add very little, considering the model presented already provides very good accuracy using clinical data and is better than predictive models to date [30,32,48].

While basis-function methods yield reasonably accurate V_{frc}, PIP and PIV estimates using the single compartment model [30–32, 48,66], the virtual patient model presented is significantly more accurate in calculating these values using the more detailed mechanics model presented. Predicted V_{frc} errors average 0.018L compared to 0.093L using prior basis-function methods [66], and are

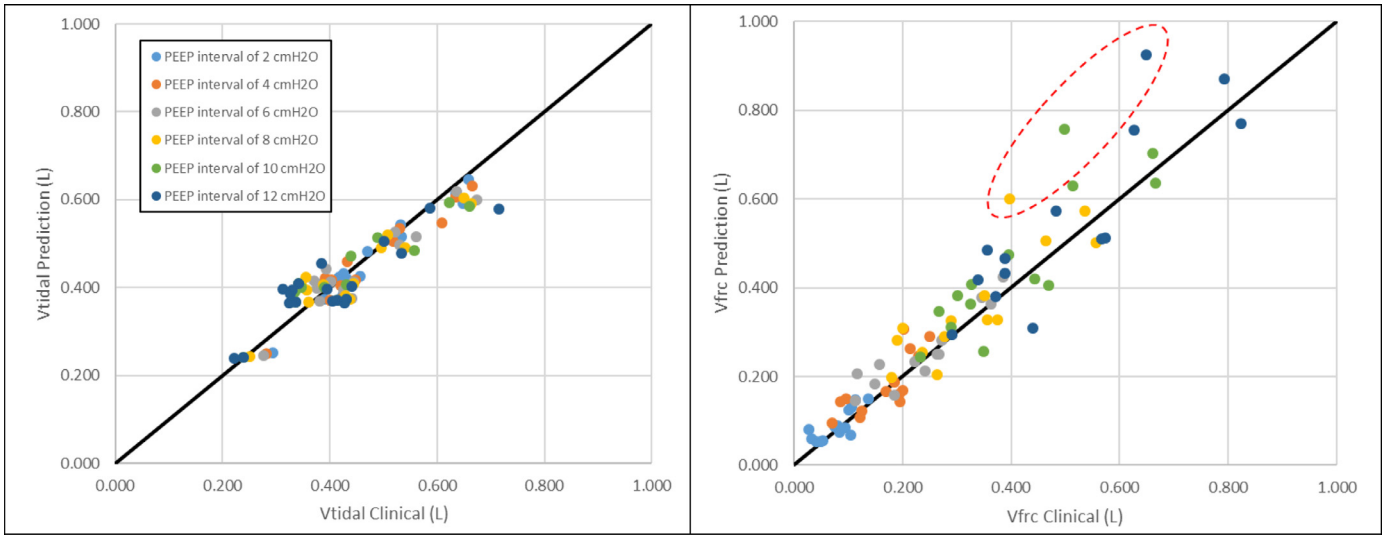

Fig. 6. Maastricht cohort prediction under PC MV for all patients and ΔPEEP prediction intervals (84 predictions). **Left**: Prediction of PIV with $R^2 = 0.86$ **Right**: Prediction of V_{frc} with $R^2 = 0.83$ or $R^2 = 0.91$ excluding 3 outliers (81 predictions) from the highest three prediction intervals for one patient.

also measurably lower for PIP and PIV. Improved accuracy and robustness increase potential clinical utility.

Clinically, V_{frc} has potential to guide care. Considering Patients 12 and 13 in Appendix B (McREM cohort), the slopes of V_{frc} over ΔPEEP intervals are very different between these patients, reflecting typical significant inter-patient variability, as seen across all patients. However, a large slope, as in Patient 13, indicates a high level of recruitability. In contrast, the low slope of Patient 12 indicates a lack of recruitability. Clinical decisions on PEEP, given this previously unavailable information, could be different because the recruited lung volume obtained by changing PEEP would now be quantified.

In particular, lung recruitability is currently broadly estimated using PEEP tests with calculations and/or imaging [67–71]. The results are neither patient-specific nor as accurate as V_{frc} predictions here. Recruitability is an open issue in Covid-19 care, as with the earlier H1N1 outbreak [69,70]. The slope of predicted model-based V_{frc} over PEEP thus offers a new and potentially more accurate approach to assess recruitability in MV patients.

The chest-lung system is considered overdamped with negligible chest wall and lung accelerations in breathing [59]. Thus, a large damping coefficient enables a steady-state simulation matching observed clinical data. While the choice of ξ is non-unique, a sensitivity analysis in Appendix E shows good prediction accuracy across a range of $\xi > 10$. Therefore, a fixed value ($\xi = 20$) should generalise well.

The proposed HLM has less nonlinearity for expiration than inspiration, producing relatively higher errors during expiration, as seen in detailed results in Appendices A-D. More complex expiration mechanics might increase the prediction accuracy for V_{frc} since this residual volume is gained during expiration. However, the ability to automate the identification of a more complex model with more parameter would be reduced. Equally, more complexity can provide greater physiological relevance, but does not guarantee improved prediction accuracy. Promising results over 32 patients in two independent trials using different MV modes indicates significant robustness, minimising this limitation.

A second limitation could be higher errors for some patients and predictions in Appendices A-D and Figs. 5 and 6. However, larger errors are not randomly distributed and occur at clinically unrealistic and large ΔPEEP intervals. They also cluster in specific patients. These errors could also be a function of the ventilator or PEEP valve, rather than the model. Equally, they occur at clinically unrealistic ΔPEEP changes, and would have no clinical impact.

Inter-disciplinarity could be a limitation or strength. The HLM derives from similar civil engineering mechanics [72–74], and the HLA elastance identification method was developed for earthquake engineering damage monitoring [49,55–58, 75–77]. These models and methods are unproven in biomedical engineering and clinical medicine applications. However, the accuracy of the results, particularly in prediction, indicates this limitation has minimal impact and the fundamental mechanics generalise well.

Finally, creating the virtual patient model requires no clinical or engineering input. It could thus be automated for real-time monitoring, decision support, and personalisation of care. Virtual patient guided care has demonstrated clinical benefit in glycemic control [78], and this model enables extension of this approach to MV.

5. Conclusions

Patient-specific digital twins or virtual patients built on clinical data and a proven nonlinear mechanics model offer accurate prediction of patient-specific lung mechanics response to changes in mechanical ventilation settings, enabling personalised, precision care to improve outcomes and cost. The model and method developed provide very good prediction accuracy, as well as mechanical and clinical insight not previously available and not provided by data-driven methods or less complex models. There is also the potential to merge the developed underlying mechanical model and machine learning using patient-specific and breath-specific data generated by the model. Overall, this work provides a very promising proof-of-concept, validated across multiple patients and ventilation modes.

Declaration of Competing Interest

The authors declare that they have no conflict of interest.

Acknowledgements

This work was supported by the NZ Tertiary Education Commission (TEC) fund MedTech CoRE (Centre of Research Excellence; #3705718) and the NZ National Science Challenge 7, Science for Technology and Innovation (2019-S3-CRS). The authors also acknowledge support from the EU H2020 R&I programme (MSCA-RISE-2019 call) under grant agreement #872488 — DCPM.

Appendix A. PV loop predictions for McREM VC MV cohort (N = 18 patients)

Volume in L, Pressure in cmH_2O, PIP error in cmH_2O for Patients 1-18. Identified at PEEP1 and predicted from PEEP1 up to PEEP7 (12 cm H2O higher in 2 cmH2o increments).

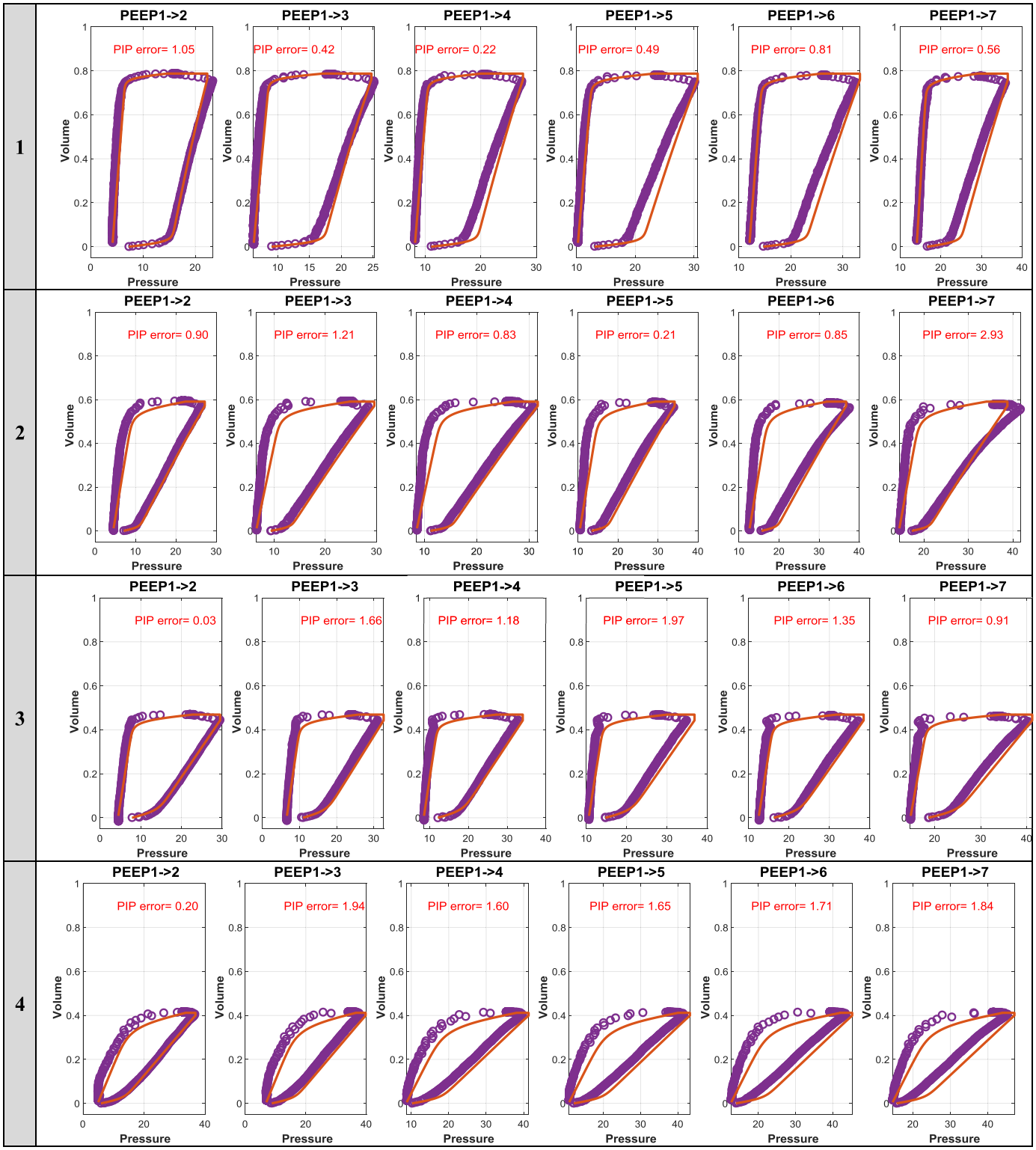

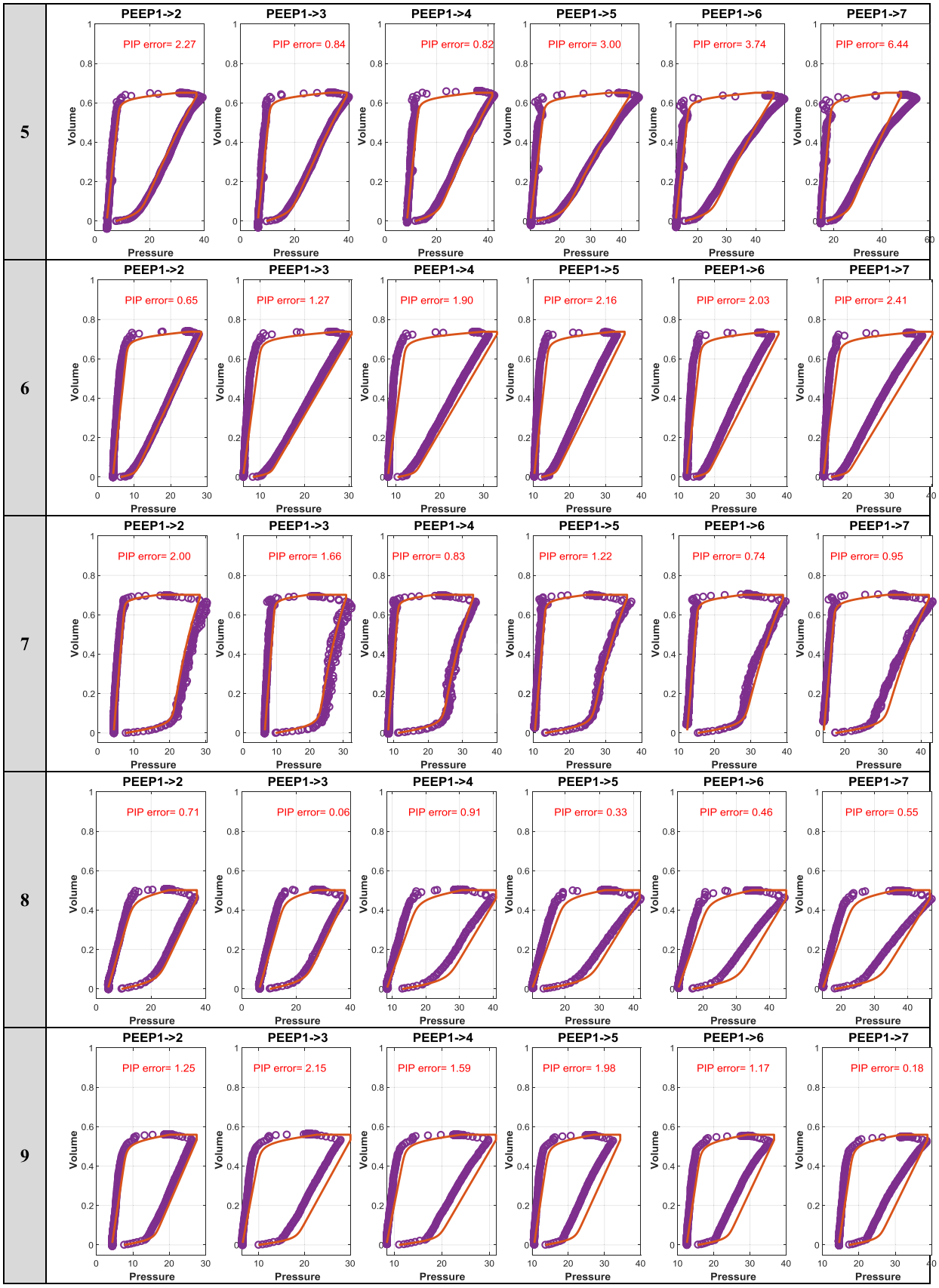
5
PEEP1->2
PIP error= 2.27
PEEP1->3
PIP error= 0.84
PEEP1->4
PIP error= 0.82
PEEP1->5
PIP error= 3.00
PEEP1->6
PIP error= 3.74
PEEP1->7
PIP error= 6.44
6
PEEP1->2
PIP error= 0.65
PEEP1->3
PIP error= 1.27
PEEP1->4
PIP error= 1.90
PEEP1->5
PIP error= 2.16
PEEP1->6
PIP error= 2.03
PEEP1->7
PIP error= 2.41
7
PEEP1->2
PIP error= 2.00
PEEP1->3
PIP error= 1.66
PEEP1->4
PIP error= 0.83
PEEP1->5
PIP error= 1.22
PEEP1->6
PIP error= 0.74
PEEP1->7
PIP error= 0.95
8
PEEP1->2
PIP error= 0.71
PEEP1->3
PIP error= 0.06
PEEP1->4
PIP error= 0.91
PEEP1->5
PIP error= 0.33
PEEP1->6
PIP error= 0.46
PEEP1->7
PIP error= 0.55
9
PEEP1->2
PIP error= 1.25
PEEP1->3
PIP error= 2.15
PEEP1->4
PIP error= 1.59
PEEP1->5
PIP error= 1.98
PEEP1->6
PIP error= 1.17
PEEP1->7
PIP error= 0.18
Volume
Pressure

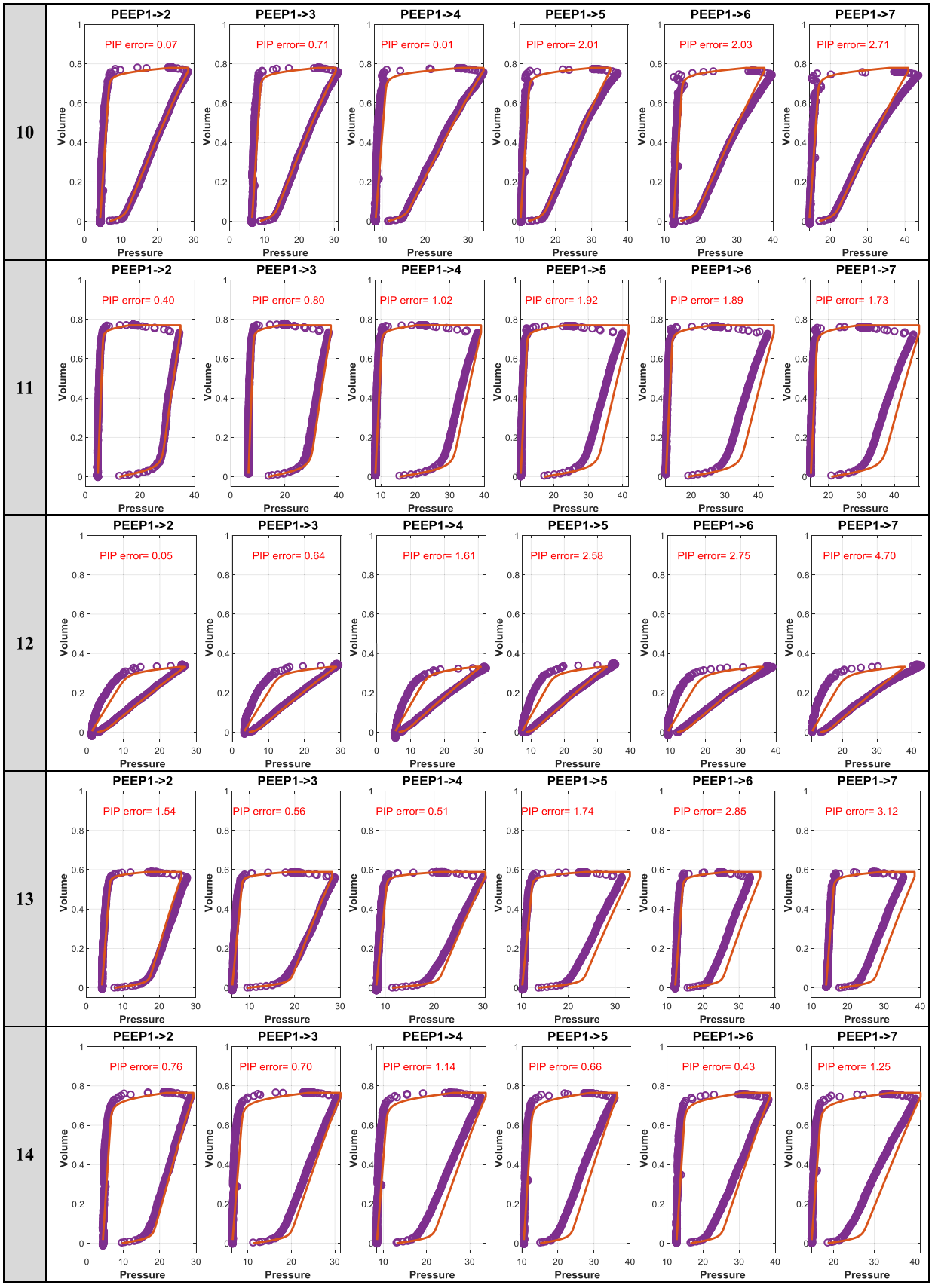
10
PEEP1->2
PIP error= 0.07
PEEP1->3
PIP error= 0.71
PEEP1->4
PIP error= 0.01
PEEP1->5
PIP error= 2.01
PEEP1->6
PIP error= 2.03
PEEP1->7
PIP error= 2.71
11
PEEP1->2
PIP error= 0.40
PEEP1->3
PIP error= 0.80
PEEP1->4
PIP error= 1.02
PEEP1->5
PIP error= 1.92
PEEP1->6
PIP error= 1.89
PEEP1->7
PIP error= 1.73
12
PEEP1->2
PIP error= 0.05
PEEP1->3
PIP error= 0.64
PEEP1->4
PIP error= 1.61
PEEP1->5
PIP error= 2.58
PEEP1->6
PIP error= 2.75
PEEP1->7
PIP error= 4.70
13
PEEP1->2
PIP error= 1.54
PEEP1->3
PIP error= 0.56
PEEP1->4
PIP error= 0.51
PEEP1->5
PIP error= 1.74
PEEP1->6
PIP error= 2.85
PEEP1->7
PIP error= 3.12
14
PEEP1->2
PIP error= 0.76
PEEP1->3
PIP error= 0.70
PEEP1->4
PIP error= 1.14
PEEP1->5
PIP error= 0.66
PEEP1->6
PIP error= 0.43
PEEP1->7
PIP error= 1.25
Volume
Pressure

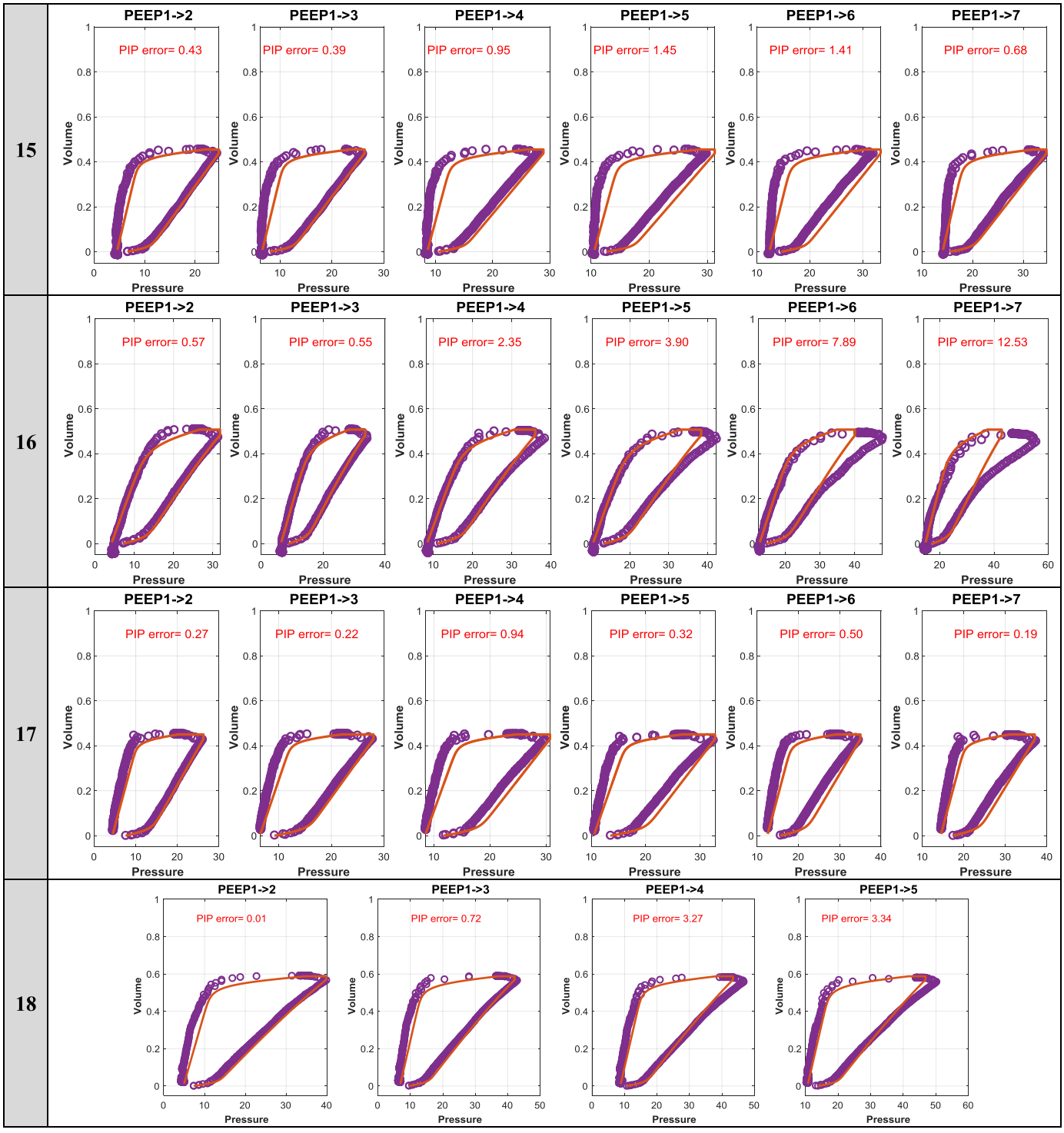
15
PEEP1->2
PIP error= 0.43
PEEP1->3
PIP error= 0.39
PEEP1->4
PIP error= 0.95
PEEP1->5
PIP error= 1.45
PEEP1->6
PIP error= 1.41
PEEP1->7
PIP error= 0.68
16
PEEP1->2
PIP error= 0.57
PEEP1->3
PIP error= 0.55
PEEP1->4
PIP error= 2.35
PEEP1->5
PIP error= 3.90
PEEP1->6
PIP error= 7.89
PEEP1->7
PIP error= 12.53
17
PEEP1->2
PIP error= 0.27
PEEP1->3
PIP error= 0.22
PEEP1->4
PIP error= 0.94
PEEP1->5
PIP error= 0.32
PEEP1->6
PIP error= 0.50
PEEP1->7
PIP error= 0.19
18
PEEP1->2
PIP error= 0.01
PEEP1->3
PIP error= 0.72
PEEP1->4
PIP error= 3.27
PEEP1->5
PIP error= 3.34
Volume
Pressure

Appendix B. Accumulated V_{frc} prediction for McREM VC MV cohort (N=18 patients)

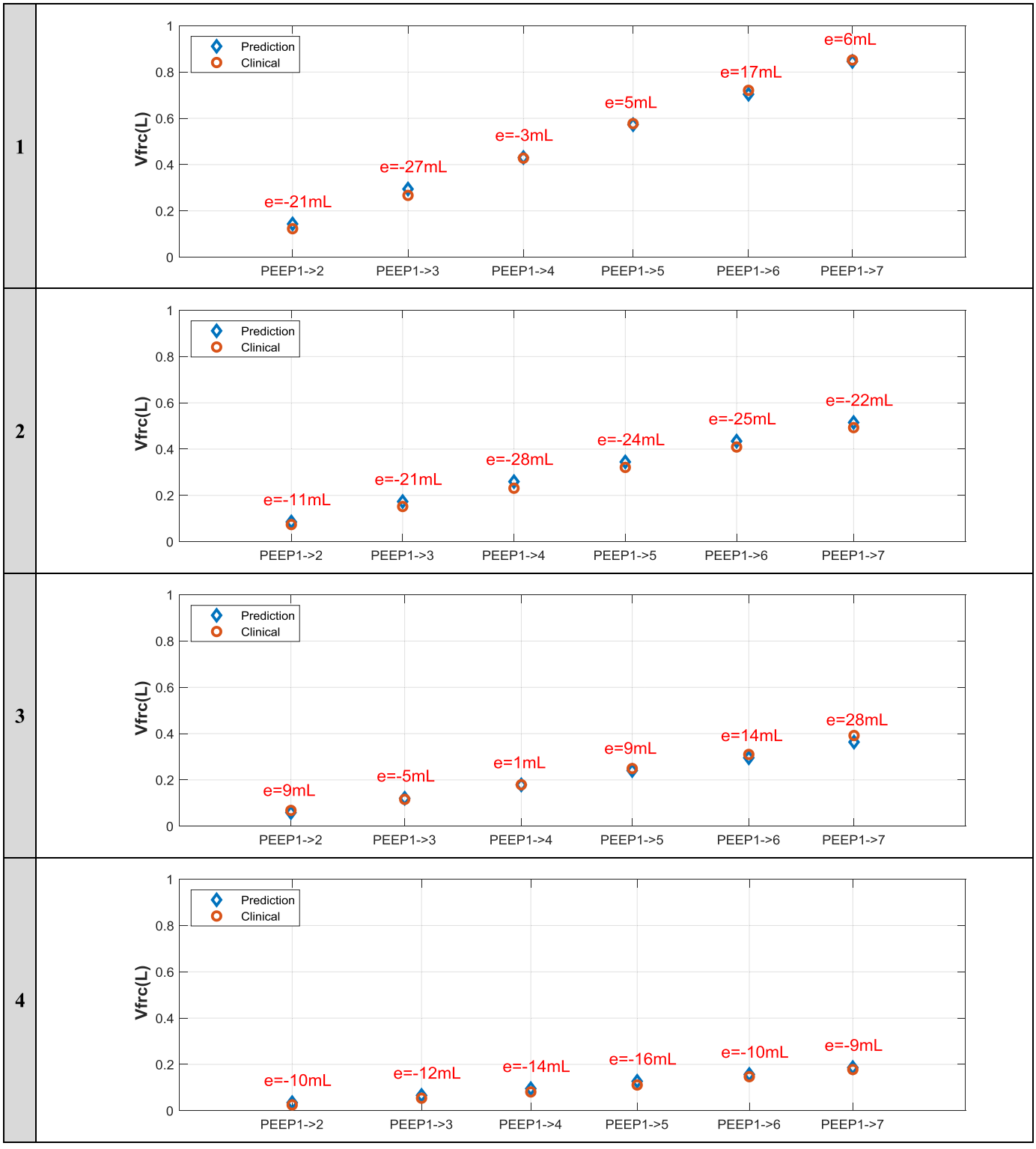

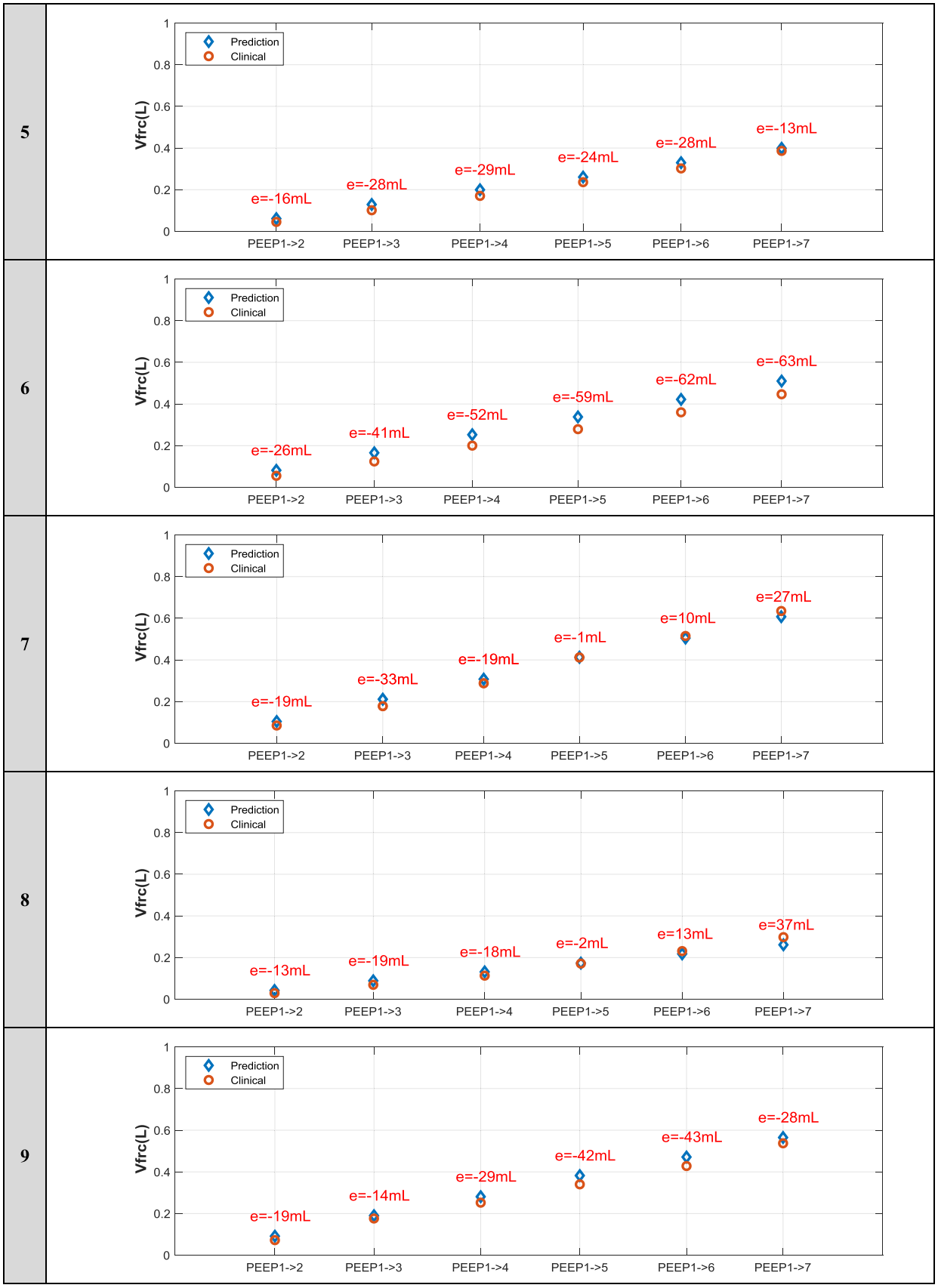
5
Prediction
Clinical
Vfrc(L)
e=-16mL
e=-28mL
e=-29mL
e=-24mL
e=-28mL
e=-13mL
PEEP1->2
PEEP1->3
PEEP1->4
PEEP1->5
PEEP1->6
PEEP1->7
6
Prediction
Clinical
Vfrc(L)
e=-26mL
e=-41mL
e=-52mL
e=-59mL
e=-62mL
e=-63mL
PEEP1->2
PEEP1->3
PEEP1->4
PEEP1->5
PEEP1->6
PEEP1->7
7
Prediction
Clinical
Vfrc(L)
e=-19mL
e=-33mL
e=-19mL
e=-1mL
e=10mL
e=27mL
PEEP1->2
PEEP1->3
PEEP1->4
PEEP1->5
PEEP1->6
PEEP1->7
8
Prediction
Clinical
Vfrc(L)
e=-13mL
e=-19mL
e=-18mL
e=-2mL
e=13mL
e=37mL
PEEP1->2
PEEP1->3
PEEP1->4
PEEP1->5
PEEP1->6
PEEP1->7
9
Prediction
Clinical
Vfrc(L)
e=-19mL
e=-14mL
e=-29mL
e=-42mL
e=-43mL
e=-28mL
PEEP1->2
PEEP1->3
PEEP1->4
PEEP1->5
PEEP1->6
PEEP1->7

10	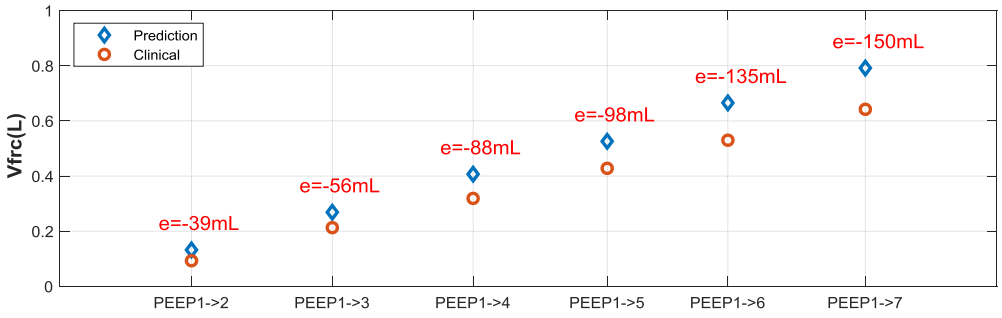
11	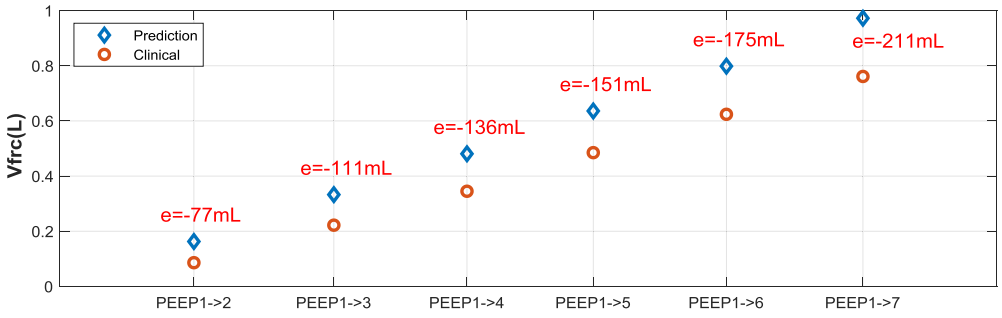
12	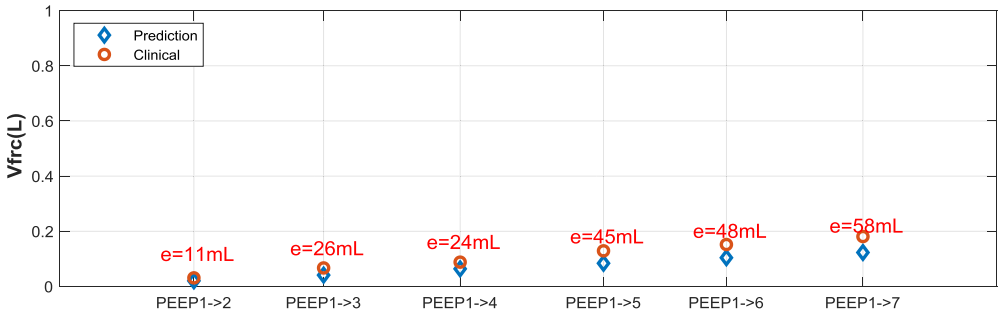
13	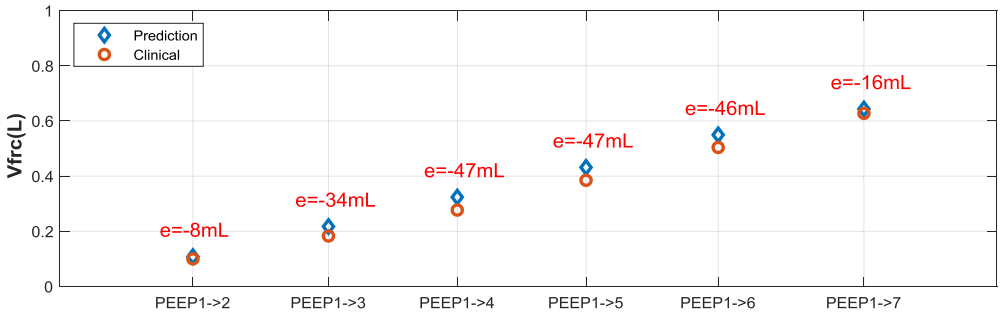
14	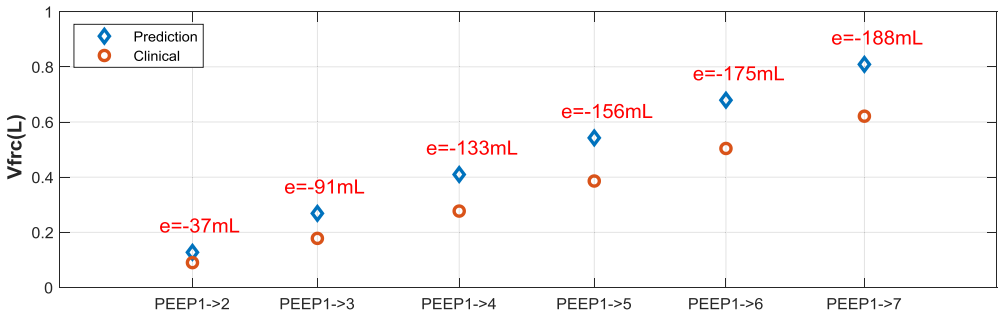

Prediction
Clinical
Vfrc(L)
PEEP1->2
PEEP1->3
PEEP1->4
PEEP1->5
PEEP1->6
PEEP1->7
e=-39mL
e=-56mL
e=-88mL
e=-98mL
e=-135mL
e=-150mL
e=-77mL
e=-111mL
e=-136mL
e=-151mL
e=-175mL
e=-211mL
e=11mL
e=26mL
e=24mL
e=45mL
e=48mL
e=58mL
e=-8mL
e=-34mL
e=-47mL
e=-47mL
e=-46mL
e=-16mL
e=-37mL
e=-91mL
e=-133mL
e=-156mL
e=-175mL
e=-188mL

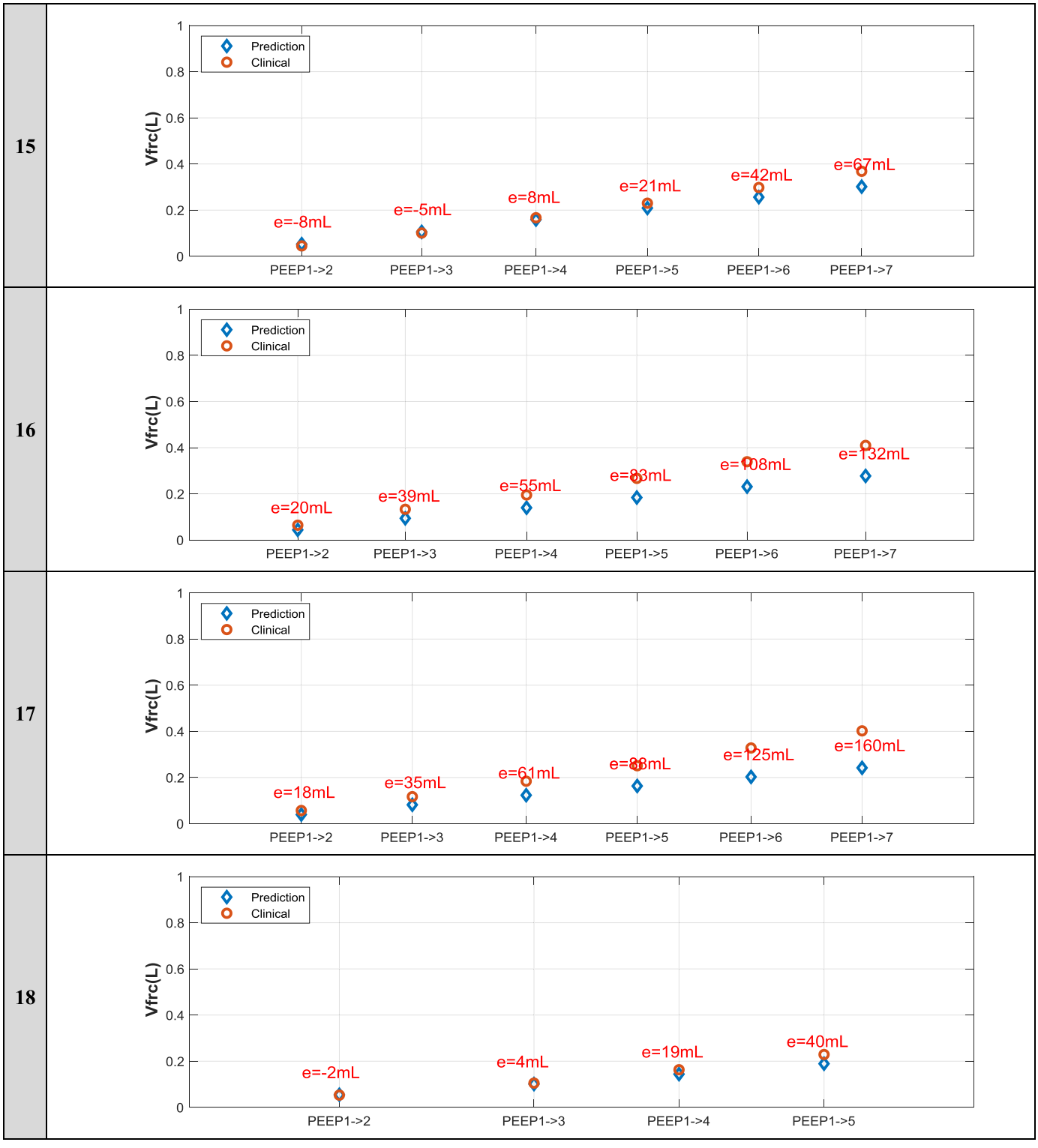
15
Prediction
Clinical
Vfrc(L)
e=-8mL
e=-5mL
e=8mL
e=21mL
e=42mL
e=67mL
PEEP1->2
PEEP1->3
PEEP1->4
PEEP1->5
PEEP1->6
PEEP1->7
16
e=20mL
e=39mL
e=55mL
e=83mL
e=108mL
e=132mL
17
e=18mL
e=35mL
e=61mL
e=88mL
e=125mL
e=160mL
18
e=-2mL
e=4mL
e=19mL
e=40mL

Appendix C. PV loop predictions for Maastricht PC MV cohort (N = 14 patients)

Volume in L, Pressure in cmH_2O, PIV error in L. Identified at PEEP1 and predicted from PEEP1 up to PEEP7 (12 cm H2O higher in 2 cmH2O increments).

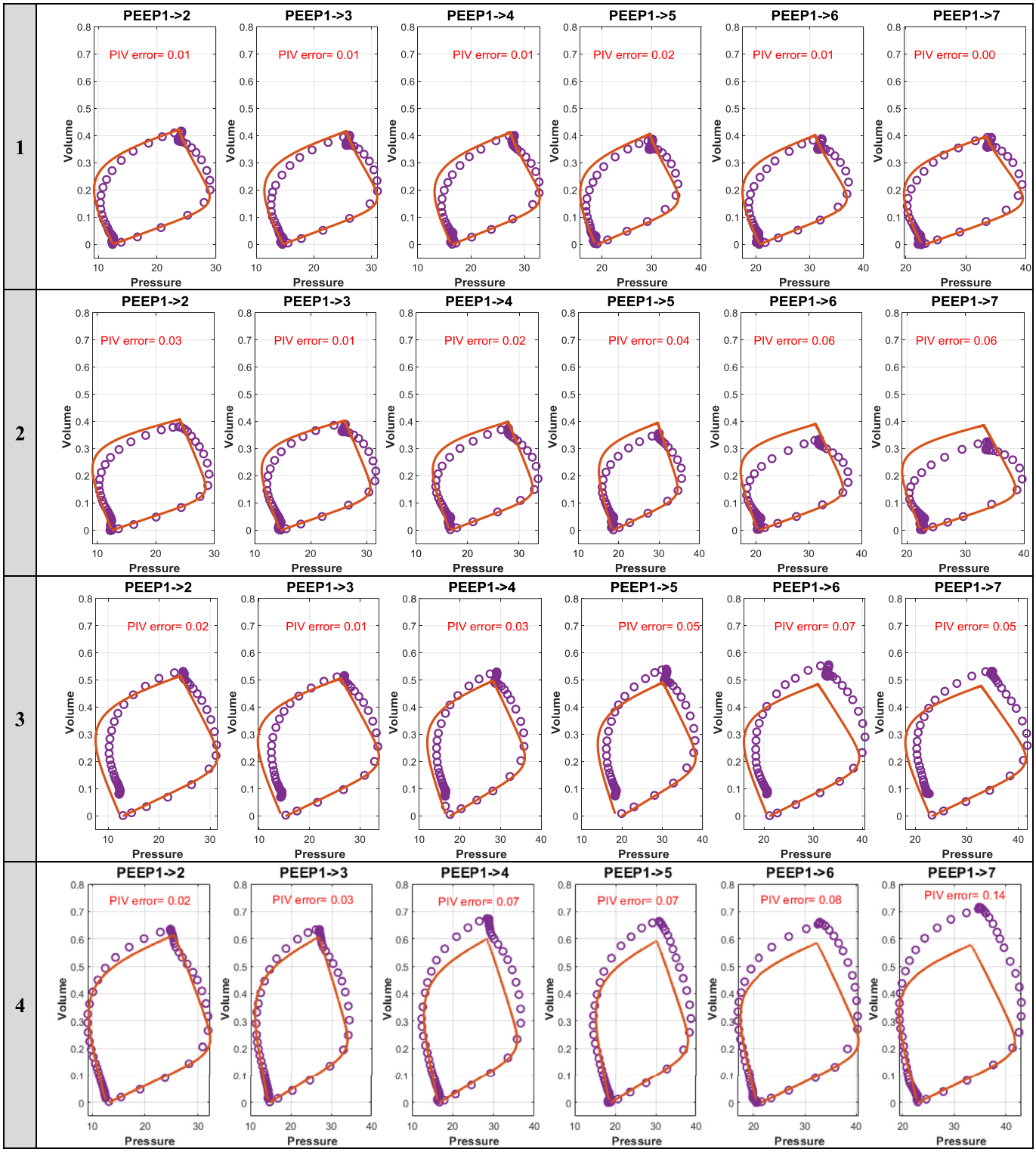

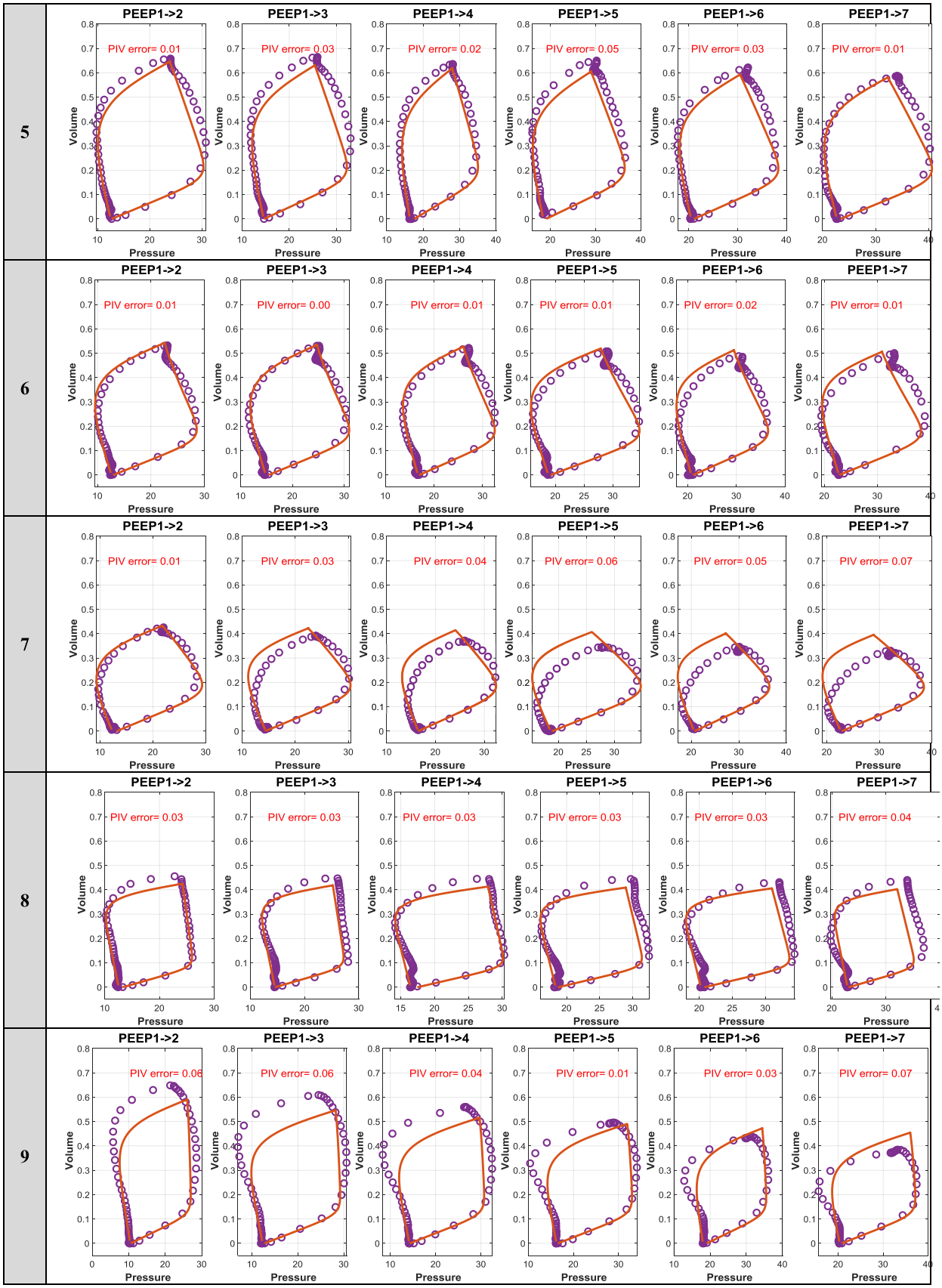
5
PEEP1->2
PIV error= 0.01
PEEP1->3
PIV error= 0.03
PEEP1->4
PIV error= 0.02
PEEP1->5
PIV error= 0.05
PEEP1->6
PIV error= 0.03
PEEP1->7
PIV error= 0.01
6
PEEP1->2
PIV error= 0.01
PEEP1->3
PIV error= 0.00
PEEP1->4
PIV error= 0.01
PEEP1->5
PIV error= 0.01
PEEP1->6
PIV error= 0.02
PEEP1->7
PIV error= 0.01
7
PEEP1->2
PIV error= 0.01
PEEP1->3
PIV error= 0.03
PEEP1->4
PIV error= 0.04
PEEP1->5
PIV error= 0.06
PEEP1->6
PIV error= 0.05
PEEP1->7
PIV error= 0.07
8
PEEP1->2
PIV error= 0.03
PEEP1->3
PIV error= 0.03
PEEP1->4
PIV error= 0.03
PEEP1->5
PIV error= 0.03
PEEP1->6
PIV error= 0.03
PEEP1->7
PIV error= 0.04
9
PEEP1->2
PIV error= 0.06
PEEP1->3
PIV error= 0.06
PEEP1->4
PIV error= 0.04
PEEP1->5
PIV error= 0.01
PEEP1->6
PIV error= 0.03
PEEP1->7
PIV error= 0.07
Volume
Pressure

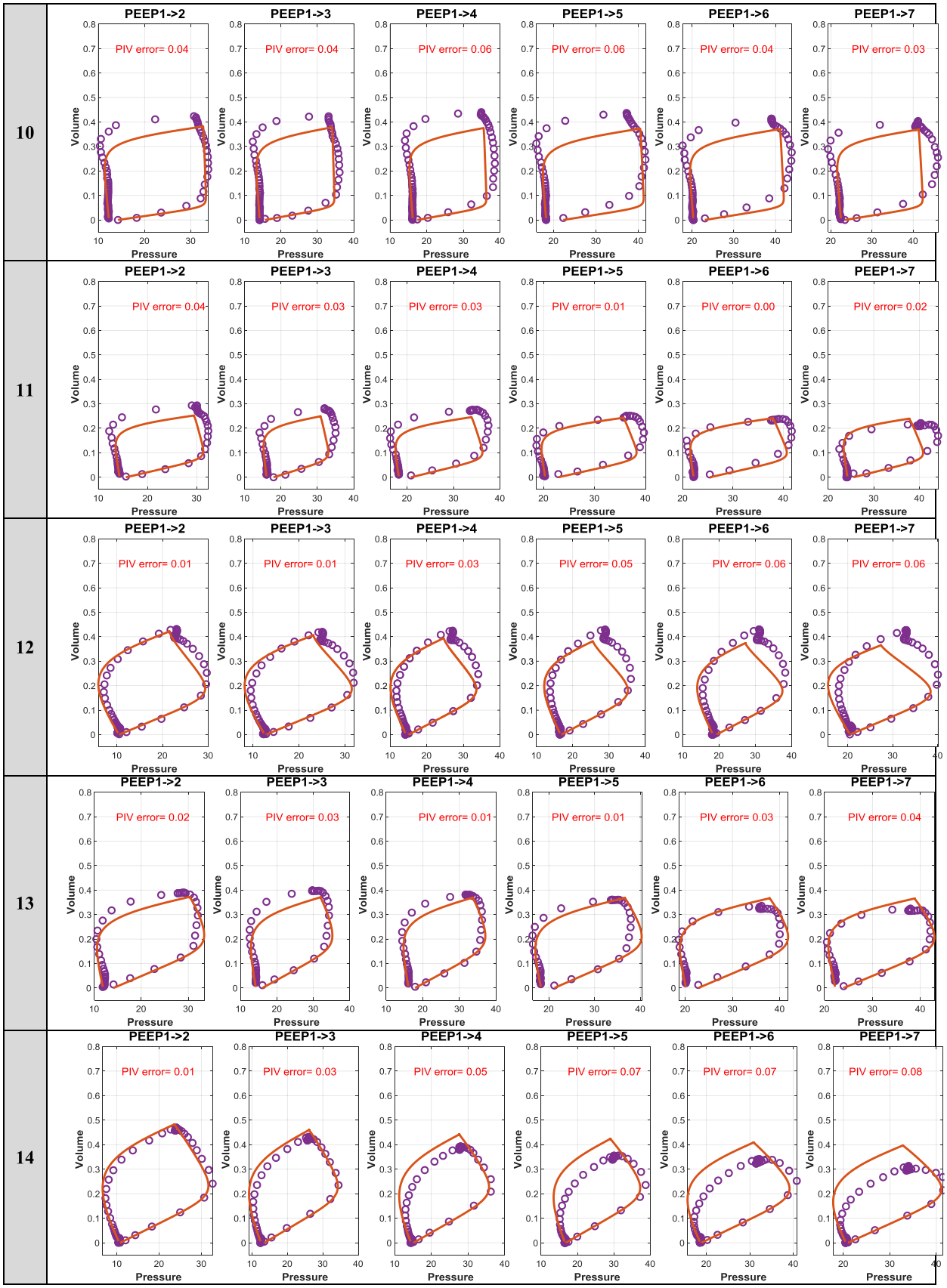
10
PEEP1->2
PIV error= 0.04
PEEP1->3
PIV error= 0.04
PEEP1->4
PIV error= 0.06
PEEP1->5
PIV error= 0.06
PEEP1->6
PIV error= 0.04
PEEP1->7
PIV error= 0.03
11
PEEP1->2
PIV error= 0.04
PEEP1->3
PIV error= 0.03
PEEP1->4
PIV error= 0.03
PEEP1->5
PIV error= 0.01
PEEP1->6
PIV error= 0.00
PEEP1->7
PIV error= 0.02
12
PEEP1->2
PIV error= 0.01
PEEP1->3
PIV error= 0.01
PEEP1->4
PIV error= 0.03
PEEP1->5
PIV error= 0.05
PEEP1->6
PIV error= 0.06
PEEP1->7
PIV error= 0.06
13
PEEP1->2
PIV error= 0.02
PEEP1->3
PIV error= 0.03
PEEP1->4
PIV error= 0.01
PEEP1->5
PIV error= 0.01
PEEP1->6
PIV error= 0.03
PEEP1->7
PIV error= 0.04
14
PEEP1->2
PIV error= 0.01
PEEP1->3
PIV error= 0.03
PEEP1->4
PIV error= 0.05
PEEP1->5
PIV error= 0.07
PEEP1->6
PIV error= 0.07
PEEP1->7
PIV error= 0.08
Volume
Pressure

Appendix D. Accumulated V_{frc} prediction for Maastricht PC MV cohort (N = 14 patients)

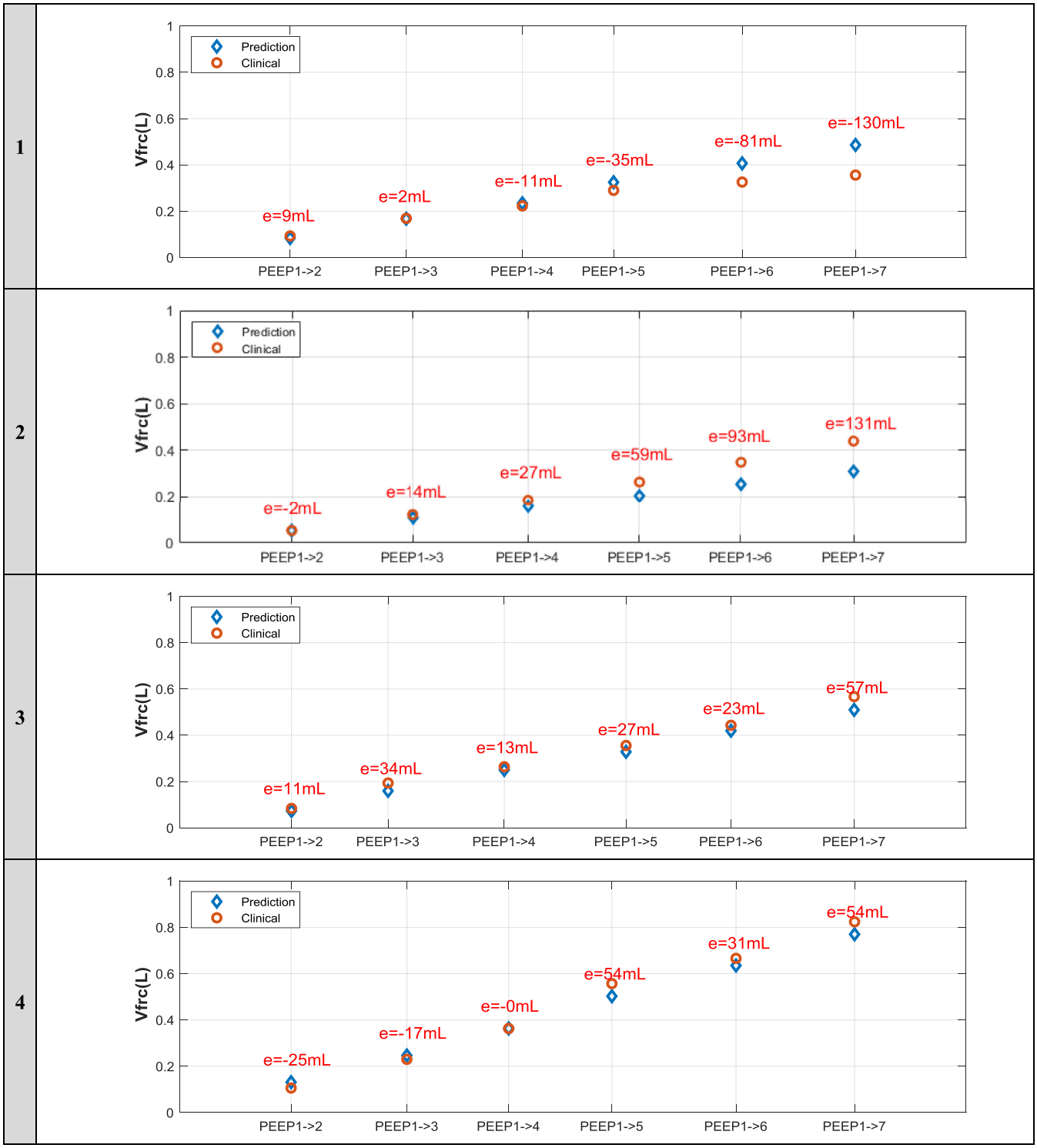

5	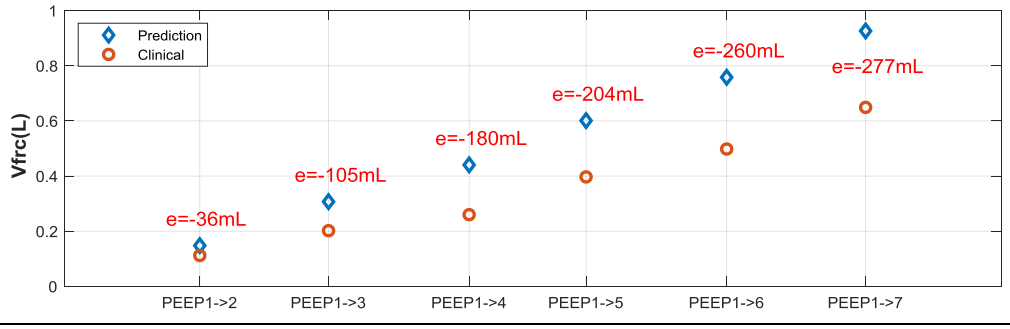
6	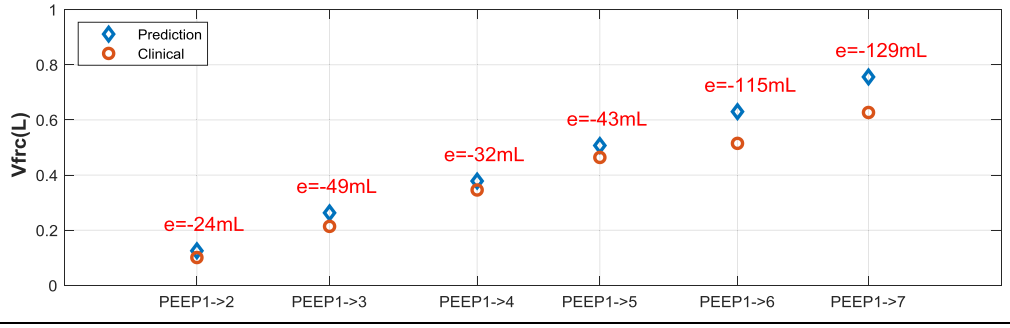
7	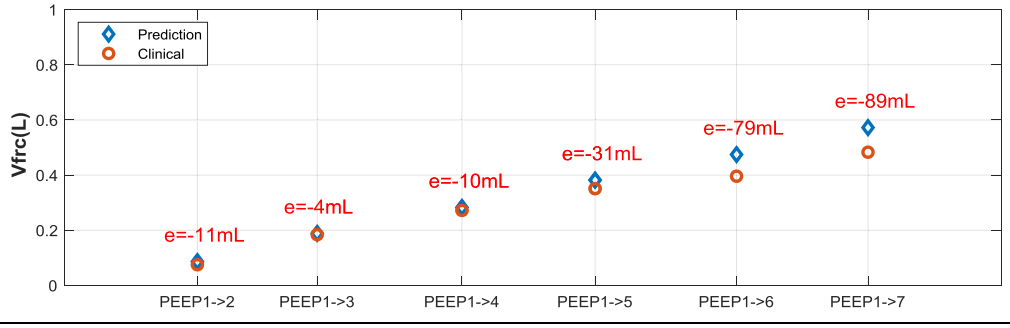
8	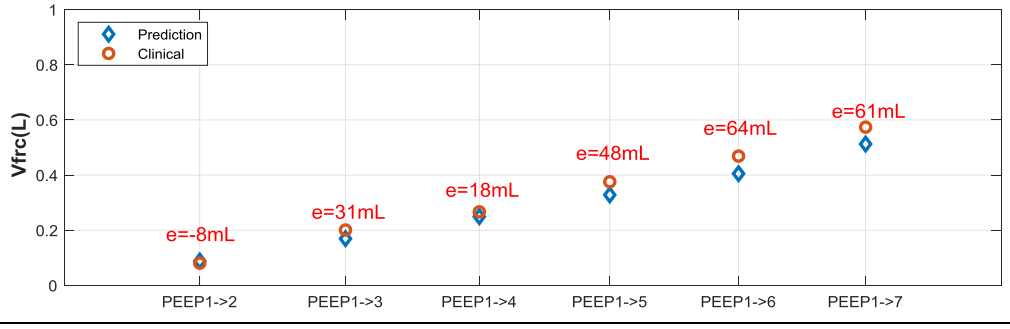
9	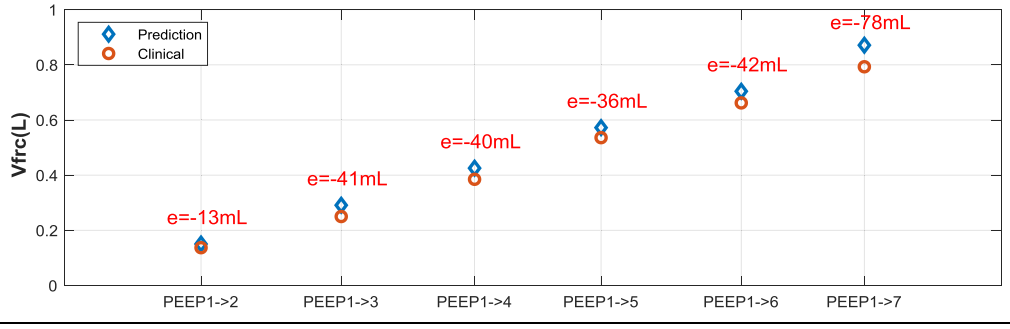

Prediction
Clinical
Vfrc(L)
PEEP1->2
PEEP1->3
PEEP1->4
PEEP1->5
PEEP1->6
PEEP1->7
e=-36mL
e=-105mL
e=-180mL
e=-204mL
e=-260mL
e=-277mL
e=-24mL
e=-49mL
e=-32mL
e=-43mL
e=-115mL
e=-129mL
e=-11mL
e=-4mL
e=-10mL
e=-31mL
e=-79mL
e=-89mL
e=-8mL
e=31mL
e=18mL
e=48mL
e=64mL
e=61mL
e=-13mL
e=-41mL
e=-40mL
e=-36mL
e=-42mL
e=-78mL

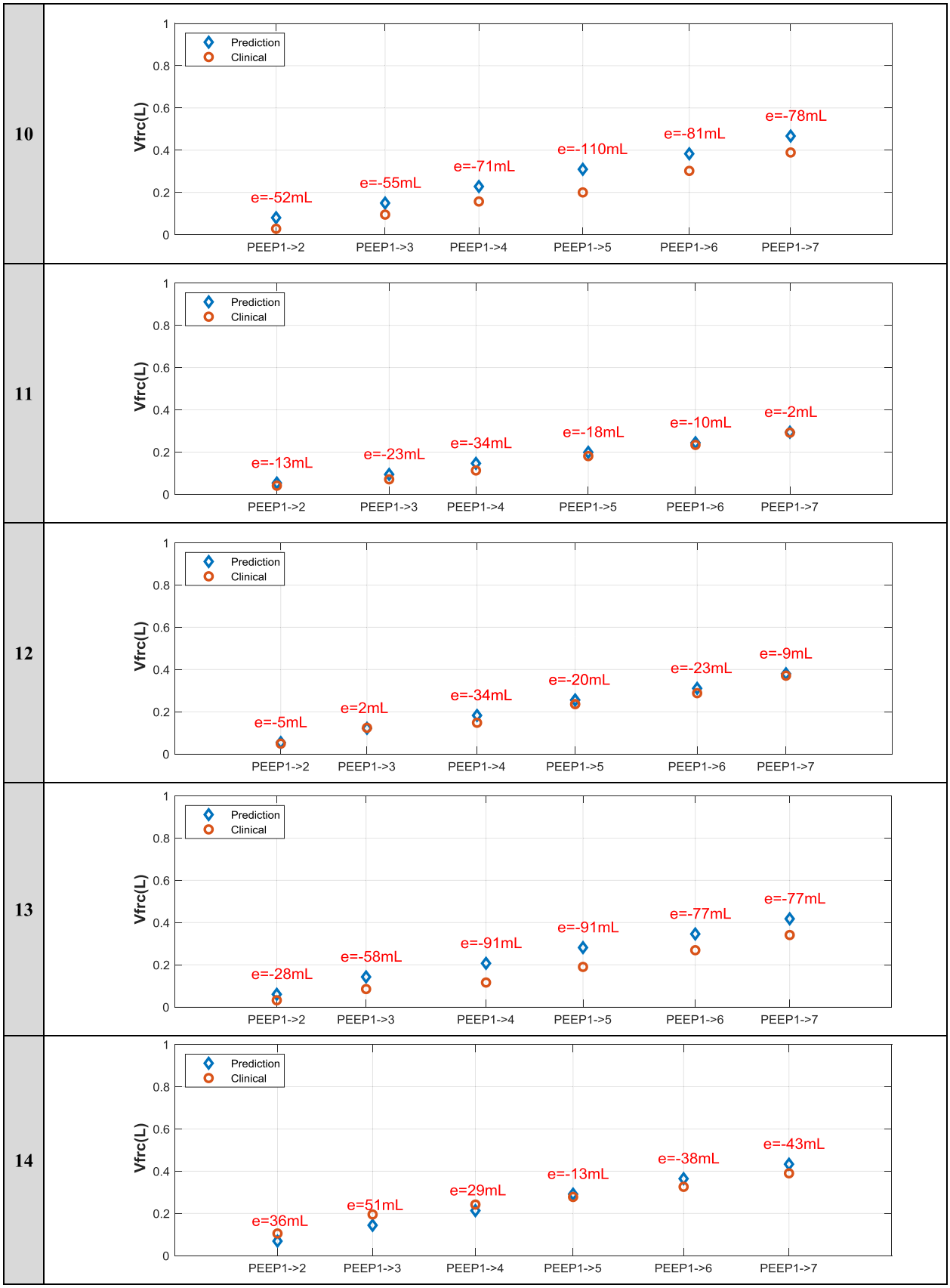
10
Prediction
Clinical
Vfrc(L)
e=-52mL
e=-55mL
e=-71mL
e=-110mL
e=-81mL
e=-78mL
PEEP1->2
PEEP1->3
PEEP1->4
PEEP1->5
PEEP1->6
PEEP1->7
11
Prediction
Clinical
Vfrc(L)
e=-13mL
e=-23mL
e=-34mL
e=-18mL
e=-10mL
e=-2mL
PEEP1->2
PEEP1->3
PEEP1->4
PEEP1->5
PEEP1->6
PEEP1->7
12
Prediction
Clinical
Vfrc(L)
e=-5mL
e=2mL
e=-34mL
e=-20mL
e=-23mL
e=-9mL
PEEP1->2
PEEP1->3
PEEP1->4
PEEP1->5
PEEP1->6
PEEP1->7
13
Prediction
Clinical
Vfrc(L)
e=-28mL
e=-58mL
e=-91mL
e=-91mL
e=-77mL
e=-77mL
PEEP1->2
PEEP1->3
PEEP1->4
PEEP1->5
PEEP1->6
PEEP1->7
14
Prediction
Clinical
Vfrc(L)
e=36mL
e=51mL
e=29mL
e=-13mL
e=-38mL
e=-43mL
PEEP1->2
PEEP1->3
PEEP1->4
PEEP1->5
PEEP1->6
PEEP1->7

Appendix E. Sensitivity of Prediction to Damping Coefficient ξ

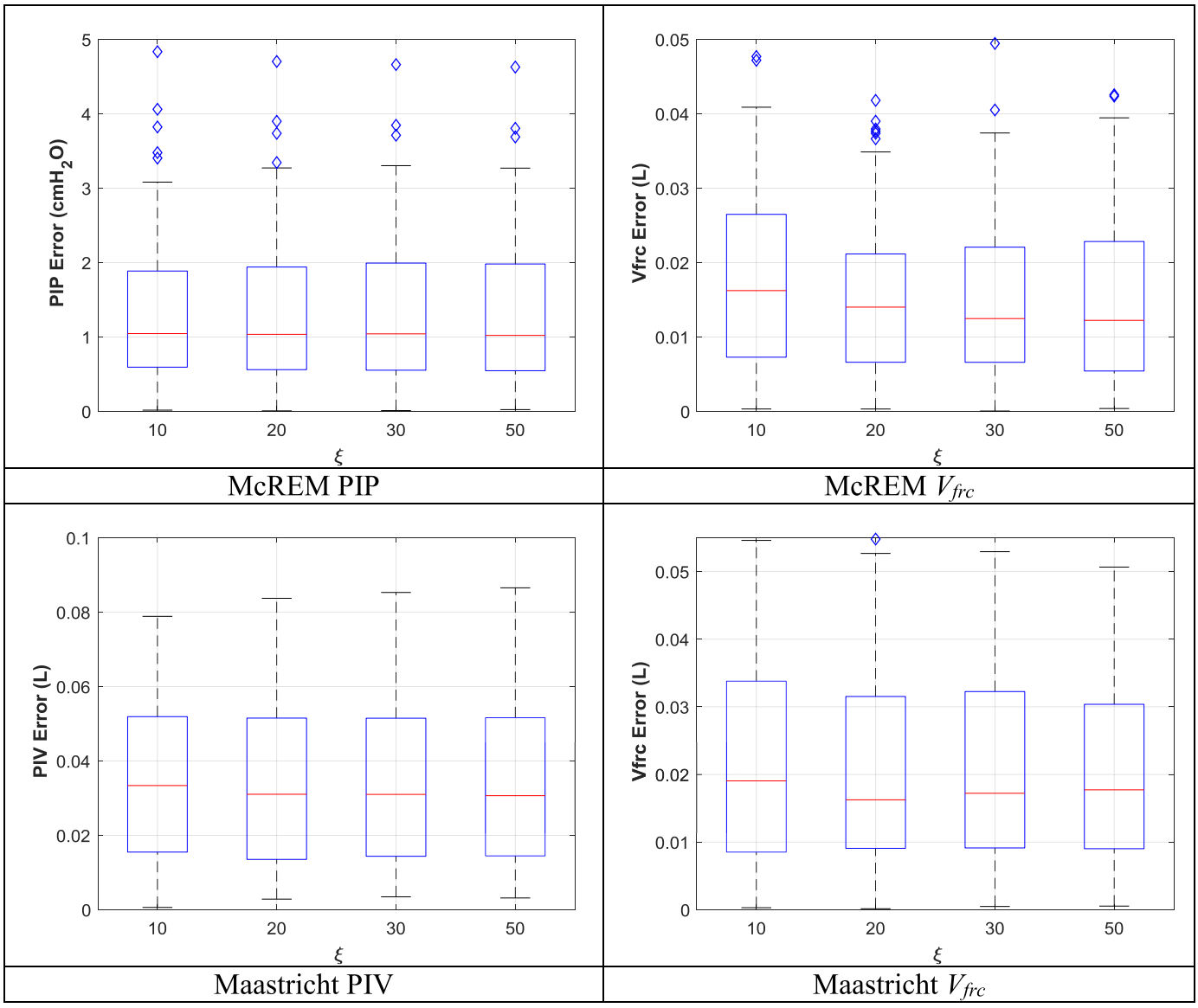

References

[1] B. Lobo, C. Hermosa, A. Abella, F. Gordo, Electrical impedance tomography, Ann. Transl. Med. 6 (2018).

[2] O. Gajic, S.I. Dara, J.L. Mendez, A.O. Adesanya, E. Festic, S.M. Caples, R. Rana, J.L.S. Sauver, J.F. Lymp, B Afessa, Ventilator-associated lung injury in patients without acute lung injury at the onset of mechanical ventilation, Crit. Care Med. 32 (2004) 1817–1824.

[3] J. Villar, Ventilator or physician-induced lung injury, Minerva Anestesiol. 71 (2005) 255 - 258.

[4] D. Carney, J. DiRocco, G. Nieman, Dynamic alveolar mechanics and ventilator-induced lung injury, Crit. Care Med. 33 (2005) S122–S128.

[5] J.M. Halter, J.M. Steinberg, H.J. Schiller, M. DaSilva, L.A. Gatto, S. Landas, G.F. Nieman, Positive end-expiratory pressure after a recruitment maneuver prevents both alveolar collapse and recruitment/derecruitment, Am. J. Respir. Crit. Care Med. 167 (2003) 1620–1626.

[6] D.R. Hess, Recruitment maneuvers and PEEP titration, Respir. Care 60 (2015) 1688–1704.

[7] A. Sundaresan, J.G. Chase, Positive end expiratory pressure in patients with acute respiratory distress syndrome–The past, present and future, Biomed. Signal Process. Control 7 (2012) 93–103.

[8] L.D. Bos, I. Martin-Loeches, M.J. Schultz, ARDS: challenges in patient care and frontiers in research, Eur. Respir. Rev. (2018) 27.

[9] J.J. Rouby, Q. Lu, I. Goldstein, Selecting the right level of positive end-expiratory pressure in patients with acute respiratory distress syndrome, Am. J. Respir. Crit. Care Med. 165 (2002) 1182–1186.

[10] A.R.D.S Network, Ventilation with lower tidal volumes as compared with traditional tidal volumes for acute lung injury and the acute respiratory distress syndrome, New Engl. J. Med. 342 (2000) 1301–1308.

[11] M.B.P. Amato, C.S.V. Barbas, D.M. Medeiros, R.B. Magaldi, G.P. Schettino, G. Lorenzi-Filho, R.A. Kairalla, D. Deheinzelin, C. Munoz, R. Oliveira, T.Y. Takagaki, C.R.R Carvalho, Effect of a protective-ventilation strategy on mortality in the acute respiratory distress syndrome, N Engl. J. Med. 338 (1998) 347–354.

[12] V.J. Major, Y.S. Chiew, G.M. Shaw, J.G. Chase, Biomedical engineer's guide to the clinical aspects of intensive care mechanical ventilation, Biomed. Eng. Onl. 17 (2018) 169, doi:10.1186/s12938-018-0599-9.

[13] A. Malhotra, Low-tidal-volume ventilation in the acute respiratory distress syndrome, N Engl J Med 357 (2007) 1113–1120, doi:10.1056/NEJMct074213.

[14] G. Bellani, L. Guerra, G. Musch, A. Zanella, N. Patroniti, T. Mauri, C. Messa, A. Pesenti, Lung regional metabolic activity and gas volume changes induced by tidal ventilation in patients with acute lung injury, Am. J. Respir. Crit. Care Med. 183 (2011) 1193–1199.

[15] P. Terragni, G. Rosboch, A. Lisi, A. Viale, V.M. Ranieri, How respiratory system mechanics may help in minimising ventilator-induced lung injury in ARDS patients, Eur. Respir. J. 22 (2003) 15s–21s.

[16] M.B. Amato, M.O. Meade, A.S. Slutsky, L. Brochard, E.L. Costa, D.A. Schoenfeld, T.E. Stewart, M. Briel, D. Talmor, A. Mercat, Driving pressure and survival in the acute respiratory distress syndrome, New Engl. J. Med. 372 (2015) 747–755.

[17] A. Protti, D.T. Andreis, M. Monti, A. Santini, C.C. Sparacino, T. Langer, E. Votta, S. Gatti, L. Lombardi, O. Leopardi, Lung stress and strain during mechanical ventilation: any difference between statics and dynamics? Crit. Care Med. 41 (2013) 1046–1055.

[18] S.V. Jain, M. Kollisch-Singule, J. Satalin, Q. Searles, L. Dombert, O. Abdel-Razek, N. Yepuri, A. Leonard, A. Gruessner, P. Andrews, The role of high airway pressure and dynamic strain on ventilator-induced lung injury in a heterogeneous acute lung injury model, Intens. Care Med. Exp. 5 (2017) 25.

[19] M. Briel, M. Meade, A. Mercat, R.G. Brower, D. Talmor, S.D. Walter, A.S. Slutsky, E. Pullenayegum, Q. Zhou, D. Cook, Higher vs lower positive end-expiratory pressure in patients with acute lung injury and acute respiratory distress syndrome: systematic review and meta-analysis, Jama 303 (2010) 865–873.

[20] A.B. Cavalcanti, É.A. Suzumura, L.N. Laranjeira, D. de Moraes Paisani, L.P. Damiani, H.P. Guimarães, E.R. Romano, M. de Moraes Regenga, L.N.T. Taniguchi, C Teixeira, Effect of lung recruitment and titrated positive end-expiratory pressure (PEEP) vs low PEEP on mortality in patients with acute respiratory distress syndrome: a randomized clinical trial, Jama 318 (2017) 1335–1345.

[21] J.G. Chase, J.C. Preiser, J.L. Dickson, A. Pironet, Y.S. Chiew, C.G. Pretty, G.M. Shaw, B. Benyo, K. Moeller, S. Safaei, M. Tawhai, P. Hunter, T. Desaive, Next-generation, personalised, model-based critical care medicine: a state-of-the art review of in silico virtual patient models, methods, and cohorts, and how to validation them, Biomed. Eng. Onl. 17 (2018) 24, doi:10.1186/s12938-018-0455-y.

[22] M. Tawhai, A. Clark, J. Chase, The lung physiome and virtual patient models: from morphometry to clinical translation, Morphologie 103 (2019) 131–138.

[23] J.F. Dasta, T.P. McLaughlin, S.H. Mody, C.T. Piech, Daily cost of an intensive care unit day: the contribution of mechanical ventilation, Crit. Care Med. 33 (2005) 1266–1271.

[24] J. Corral-Acero, F. Margara, M. Marciniak, C. Rodero, F. Loncaric, Y. Feng, A. Gilbert, J.F. Fernandes, H.A. Bukhari, A. Wajdan, The 'Digital Twin'to enable the vision of precision cardiology, Eur. Heart J. (2020).

[25] J.G. Chase, J.-C. Preiser, J.L. Dickson, A. Pironet, Y.S. Chiew, C.G. Pretty, G.M. Shaw, B. Benyo, K. Moeller, S. Safaei, Next-generation, personalised, model-based critical care medicine: a state-of-the art review of in silico virtual patient models, methods, and cohorts, and how to validation them, Biomed. Eng. Onl. 17 (2018) 1–29.

[26] R. Langdon, P.D. Docherty, C. Schranz, J.G. Chase, Prediction of high airway pressure using a non-linear autoregressive model of pulmonary mechanics, Biomed. Eng. Onl. 16 (2017) 126, doi:10.1186/s12938-017-0415-y.

[27] R. Langdon, P.D. Docherty, Y.S. Chiew, J.G. Chase, Extrapolation of a non-linear autoregressive model of pulmonary mechanics, Math. Biosci. 284 (2017) 32–39, doi:10.1016/j.mbs.2016.08.001.

[28] J.H.T. Bates, Lung Mechanics: An Inverse Modeling Approach, Cambridge University Press, 2009.

[29] J.H.T. Bates, Engineering in medicine and biology society, Ann. Int. Conf. IEEE (2009) 170–172.

[30] S.E. Morton, J.L. Knopp, J.G. Chase, K. Möller, P. Docherty, G.M. Shaw, M. Tawhai, Predictive virtual patient modelling of mechanical ventilation: impact of recruitment function, Ann. Biomed. Eng. 47 (2019) 1626–1641.

[31] S.E. Morton, J. Dickson, J.G. Chase, P. Docherty, T. Desaive, S.L. Howe, G.M. Shaw, M. Tawhai, A virtual patient model for mechanical ventilation, Comput. Methods Progr. Biomed. 165 (2018) 77–87 https://doi.org/10.1016/j.cmpb.2018.08.004.

[32] S.E. Morton, J.L. Knopp, M.H. Tawhai, P. Docherty, S.J. Heines, D.C. Bergmans, K. Möller, J.G. Chase, Prediction of lung mechanics throughout recruitment maneuvers in pressure-controlled ventilation, Comput. Methods Progr. Biomed. (2020) 105696.

[33] S.B. Jawde, A.J. Walkey, A. Majumdar, G.T. O'Connor, B.J. Smith, J.H. Bates, K.R. Lutchen, B. Suki, tracking respiratory mechanics around natural breathing rates via variable ventilation, Sci. Rep. 10 (2020) 1–12.

[34] K.L. Hamlington, B.J. Smith, G.B. Allen, J.H. Bates, Predicting ventilator-induced lung injury using a lung injury cost function, J. Appl. Physiol. 121 (2016) 106–114.

[35] B. Ma, J. Bates, Modeling the complex dynamics of derecruitment in the lung, Ann. Biomed. Eng. 38 (2010) 3466–3477, doi:10.1007/s10439-010-0095-2.

[36] B. Ma, J.H. Bates, Continuum vs. spring network models of airway-parenchymal interdependence, J. Appl. Physiol. 113 (2012) 124–129.

[37] M.M. Mellenthin, S.A. Seong, G.S. Roy, E. Bartolák-Suki, K.L. Hamlington, J.H. Bates, B.J. Smith, Using injury cost functions from a predictive single-compartment model to assess the severity of mechanical ventilator-induced lung injuries, J. Appl. Physiol. 127 (2019) 58–70.

[38] J.H. Bates, B.J. Smith, Ventilator-induced lung injury and lung mechanics, Ann. Transl. Med. 6 (2018).

[39] Q. Sun, C. Zhou, J.G. Chase, Parameter updating of a patient-specific lung mechanics model for optimising mechanical ventilation, Biomed. Signal Process. Control (2020) 102003.

[40] J.H. Bates, G.B. Allen, The estimation of lung mechanics parameters in the presence of pathology: a theoretical analysis, Ann. Biomed. Eng. 34 (2006) 384–392.

[41] K.L. Steimle, M.L. Mogensen, D.S. Karbing, J.B. de la Serna, S. Andreassen, A model of ventilation of the healthy human lung, Comput. Methods Progr. Biomed. 101 (2011) 144–155.

[42] M.H. Tawhai, A. Pullan, P. Hunter, Generation of an anatomically based three-dimensional model of the conducting airways, Ann. Biomed. Eng. 28 (2000) 793–802.

[43] M.H. Tawhai, P. Hunter, J. Tschirren, J. Reinhardt, G. McLennan, E.A. Hoffman, CT-based geometry analysis and finite element models of the human and ovine bronchial tree, J. Appl. Physiol. 97 (2004) 2310–2321, doi:10.1152/japplphysiol.00520.2004.

[44] M.H. Tawhai, J.H.T Bates, Multi-scale lung modeling, J. Appl. Physiol. 110 (2011) 1466–1472, doi:10.1152/japplphysiol.01289.2010.

[45] K. Burrowes, J. De Backer, R. Smallwood, P. Sterk, I. Gut, R. Wirix-Speetjens, S. Siddiqui, J. Owers-Bradley, J. Wild, D. Maier, Multi-scale computational models of the airways to unravel the pathophysiological mechanisms in asthma and chronic obstructive pulmonary disease (AirPROM), Interface Focus 3 (2013) 20120057.

[46] A.-M. Lauzon, J.H. Bates, G. Donovan, M. Tawhai, J. Sneyd, M. Sanderson, A multi-scale approach to airway hyperresponsiveness: from molecule to organ, Front. Physiol. 3 (2012) 191.

[47] K. Burrowes, A. Swan, N. Warren, M. Tawhai, Towards a virtual lung: multi-scale, multi-physics modelling of the pulmonary system, Philosoph. Trans. R. Soc. A: Math. Phys. Eng. Sci. 366 (2008) 3247–3263.

[48] S.E. Morton, J.L. Knopp, J.G. Chase, P. Docherty, S.L. Howe, K. Möller, G.M. Shaw, M. Tawhai, Optimising mechanical ventilation through model-based methods and automation, Ann. Rev. Control (2019) https://doi.org/10.1016/j.arcontrol.2019.05.001.

[49] C. Zhou, J.G. Chase, A new pinched nonlinear hysteretic structural model for automated creation of digital clones in structural health monitoring, Struct. Health Monitor. (2020) 1475921720920641.

[50] P.D. Docherty, J.G. Chase, T.F. Lotz, T. Desaive, A graphical method for practical and informative identifiability analyses of physiological models: a case study of insulin kinetics and sensitivity, Biomed. Eng. Onl. 10 (2011) 39, doi:10.1186/1475-925X-10-39.

[51] C. Schranz, P.D. Docherty, Y.S. Chiew, J.G. Chase, K. Moller, Structural identifiability and practical applicability of an alveolar recruitment model for ARDS patients, IEEE Trans. Biomed. Eng. 59 (2012) 3396–3404, doi:10.1109/TBME.2012.2216526.

[52] P.D. Docherty, C. Schranz, Y.-S. Chiew, K. Möller, J.G. Chase, Reformulation of the pressure-dependent recruitment model (PRM) of respiratory mechanics, Biomed. Signal Process. Control 12 (2014) 47–53.

[53] C. Schranz, J. Kretschmer, K. Möller, in: 35th Annual International Conference of the IEEE Engineering in Medicine and Biology Society (EMBC), 2013, pp. 5220–5223. IEEE.

[54] P.D. Docherty, C. Schranz, J.G. Chase, Y.S. Chiew, K. Moller, Utility of a novel error-stepping method to improve gradient-based parameter identification by increasing the smoothness of the local objective surface: a case-study of pulmonary mechanics, Comput. Methods Progr. Biomed. 114 (2014) e70–e78, doi:10.1016/j.cmpb.2013.06.017.

[55] C. Zhou, J.G. Chase, G.W. Rodgers, H. Tomlinson, C. Xu, Physical parameter identification of structural systems with hysteretic pinching, Comput.-Aid. Civ. Infrastruct. Eng. 30 (2015) 247–262.

[56] C. Zhou, J.G. Chase, G.W. Rodgers, C. Iihoshi, Damage assessment by stiffness identification for a full-scale three-story steel moment resisting frame building subjected to a sequence of earthquake excitations, Bull. Earthq. Eng. 15 (2017) 5393–5412.

[57] C. Zhou, J.G. Chase, G.W. Rodgers, Degradation evaluation of lateral story stiffness using HLA-based deep learning networks, Adv. Eng. Inf. 39 (2019) 259–268.

[58] C. Zhou, J.G. Chase, G.W. Rodgers, Support vector machines for automated modelling of nonlinear structures using health monitoring results, Mech. Syst. Signal Process. 149 (2021) 107201.

[59] R.M. Peters, The energy cost (work) of breathing, Ann. Thorac. Surg. 7 (1969) 51–67.

[60] A.K. Chopra, *Dynamics of structures*. (Pearson education upper saddle river, NJ (2012).

[61] C.A. Stahl, K. Moller, S. Schumann, R. Kuhlen, M. Sydow, C. Putensen, J. Guttmann, Dynamic versus static respiratory mechanics in acute lung injury and acute respiratory distress syndrome, Crit. Care Med. 34 (2006) 2090–2098.

[62] V. Tsolaki, I. Siempos, E. Magira, S. Kokkoris, G.E. Zakynthinos, S. Zakynthinos, PEEP levels in COVID-19 pneumonia, Crit. Care 24 (2020) 303, doi:10.1186/s13054-020-03049-4.

[63] K.T. Kim, S. Morton, S. Howe, Y.S. Chiew, J.L. Knopp, P. Docherty, C. Pretty, T. Desaive, B. Benyo, A. Szlavecz, Model-based PEEP titration versus standard practice in mechanical ventilation: a randomised controlled trial, Trials 21 (2020) 130.

[64] A. Szlavecz, Y.S. Chiew, D. Redmond, A. Beatson, D. Glassenbury, S. Corbett, V. Major, C. Pretty, G.M. Shaw, B. Benyo, T. Desaive, J.G. Chase, The clinical utilisation of respiratory elastance software (CURE Soft): a bedside software for real-time respiratory mechanics monitoring and mechanical ventilation management, Biomed. Eng. OnLine 13 (2014) 140, doi:10.1186/1475-925X-13-140.

[65] C. Zhou, J.G. Chase, G.W. Rodgers, C. Xu, Comparing model-based adaptive LMS filters and a model-free hysteresis loop analysis method for structural health monitoring, Mech. Syst. Signal Process. 84 (2017) 384–398.

[66] S.E. Morton, *Development of Virtual Patients for use in Mechanical Ventilation* Doctor of Philosophy thesis, University of Canterbury, 2019.

[67] P. Caironi, E. Carlesso, M. Cressoni, D. Chiumello, O. Moerer, C. Chiurazzi, M. Brioni, N. Bottino, M. Lazzerini, G. Bugedo, Lung recruitability is better estimated according to the Berlin definition of acute respiratory distress syndrome at standard 5 cm H2O rather than higher positive end-expiratory pressure: a retrospective cohort study, Crit. Care Med. 43 (2015) 781–790.

[68] G.F. de Matos, F. Stanzani, R.H. Passos, M.F. Fontana, R. Albaladejo, R.E. Caserta, D.C. Santos, J.B. Borges, M.B. Amato, C.S. Barbas, How large is the lung recruitability in early acute respiratory distress syndrome: a prospective case series of patients monitored by computed tomography, Crit. Care 16 (2012) R4.

[69] C. Pan, L. Chen, C. Lu, W. Zhang, J.-A. Xia, M.C. Sklar, B. Du, L. Brochard, H. Qiu, Lung recruitability in COVID-19–associated acute respiratory distress syndrome: a single-center observational study, Am. J. Respir. Crit. Care Med. 201 (2020) 1294–1297.
[70] D. Chiumello, A. Marino, M. Lazzerini, M. Caspani, L. Gattinoni, Lung recruitability in ARDS H1N1 patients, Intens. Care Med. 36 (2010) 1791–1792.
[71] E.L. Costa, J.B. Borges, A. Melo, F. Suarez-Sipmann, C. Toufen, S.H. Bohm, M.B. Amato, Bedside estimation of recruitable alveolar collapse and hyperdistension by electrical impedance tomography, Intens. Care Med. 35 (2009) 1132–1137.
[72] T.T. Baber, M.N. Noori, Random vibration of degrading, pinching systems, J. Eng. Mech. 111 (1985) 1010–1026.
[73] T. Baber, M. Noori, Modelling general hysteresis behaviour and random vibration application, J. Vibration, Acoust. Stress,Reliab. Des. 108 (1986) 411–420.
[74] M. Ismail, F. Ikhouane, J. Rodellar, The hysteresis Bouc-Wen model, a survey, Arch. Comput. Methods Eng. 16 (2009) 161–188.
[75] C. Zhou, J.G. Chase, G.W. Rodgers, C. Xu, H. Tomlinson, Overall damage identification of flag-shaped hysteresis systems under seismic excitation, Smart Struct. Syst. 16 (2015) 163–181.
[76] C. Zhou, J.G. Chase, G.W. Rodgers, A. Kuang, S. Gutschmidt, C. Xu, Performance evaluation of cwh base isolated building during two major earthquakes in christchurch, Bull. N. Z. Soc. Earthq. 48 (2015) 264–273.
[77] C. Zhou, J.G. Chase, G.W. Rodgers, Efficient hysteresis loop analysis-based damage identification of a reinforced concrete frame structure over multiple events, J. Civ. Struct. Health Monitor. (2017) 1–16.
[78] J.G. Chase, T. Desaive, J. Bohe, M. Cnop, C. De Block, J. Gunst, R. Hovorka, P. Kalfon, J. Krinsley, E. Renard, Improving glycemic control in critically ill patients: personalized care to mimic the endocrine pancreas, Crit. Care 22 (2018) 182.